https://doi.org/10.5194/essd-2024-482
Preprint. Discussion started: 26 May 2025

Open Access Earth System Science Data Discussions

CAMELS-LUX: Highly Resolved Hydro-Meteorological and Atmospheric Data for Physiographically Characterized Catchments around Luxembourg

Judith Nijzink[1,2], Ralf Loritz[3], Laurent Gourdol[1], Davide Zoccatelli[1], Jean François Iffly[4], and Laurent Pfister[1,2]

[1]Catchment and Ecohydrology Group (CAT), Environmental Research and Innovation, Luxembourg Institute of Science and Technology (LIST), Belvaux, 4422, Luxembourg
[2]Faculty of Science, Technology and Medicine (FSTM), University of Luxembourg, Esch-sur-Alzette, 4365, Luxembourg
[3]Institute for Water and Environment, Karlsruhe Institute of Technology (KIT), Karlsruhe, 76131, Germany
[4]Observatory for Climate, Environment and Biodiversity (OCEB, Environmental Research and Innovation, Luxembourg Institute of Science and Technology (LIST), Belvaux, 4422, Luxembourg

Correspondence: Judith Nijzink (judith.nijzink@outlook.com)

Abstract. Harmonized large-sample datasets have become a central pillar of hydrological research, particularly in the machine-learning era, where data-based algorithms and machine-learning techniques are gaining increasing importance in daily life. The CAMELS-LUX dataset (Catchment Attributes and MEteorology for Large-sample Studies – LUXembourg) described here covers 56 nested catchments (0.46 km^2 - 4256.62 km^2) that contribute to the Luxembourgish stream network. While Luxembourg has a relatively homogeneous climate, the physiography varies significantly on a small scale making it a suitable study area for investigating different hydrological processes, such as runoff generation or groundwater recharge. The CAMELS-LUX dataset contains hydrological observations, meteorological data, and atmospheric reanalysis data from 2004-2021. Moreover, comprehensive physiographic catchment characteristics are provided that incorporate geology classes, land use classes, and a range of topographic indices. CAMELS-LUX is distinctive as the first dataset in the CAMELS series that offers data at three different temporal resolutions: daily, hourly, and in a 15-minute time step. Furthermore, CAMELS-LUX includes a series of flash floods in 2016 and 2018 as well as major large floods in 2010 and 2021. The extensive information contained in CAMELS-LUX is instrumental in advancing our understanding of varying discharge behaviour within Luxembourg and beyond. The CAMELS-LUX dataset has been utilized to develop and train a Long-Short-Term-Memory (LSTM) model, that simulates discharge time series, providing a benchmark for subsequent hydrological modelling efforts in the area. The model based on this dataset sufficiently reproduces hydrological rainfall-runoff dependencies and can be applied to simulate discharge in sparsely gauged basins for approximation. The CAMELS-LUX dataset is available on zenodo: https://doi.org/10.5281/zenodo.13846619 (Nijzink et al., 2024).

https://doi.org/10.5194/essd-2024-482
Preprint. Discussion started: 26 May 2025

Open Access Earth System Science Data Discussions

1 Introduction

Within recent years, data-driven models have gained increasing importance in (large-scale) hydrology. To perform well these models need to be trained on extensive datasets of high quality. With this dataset covering the Luxembourgish stream network, we contribute to international initiatives in large-sample hydrology, such as the work done around differing CAMELS datasets (Catchment Attributes and MEteorology for Large-sample Studies) that work towards the classification and regionalization of catchments trying to increase the robustness of models. So far, CAMELS datasets have been published for catchments in the USA (CAMELS, Addor et al., 2017), Chile (CAMELS-CL, Alvarez-Garreton et al., 2018), Brazil (CAMELS-BR, Chagas et al., 2020), Great-Britain (CAMELS-GB, Coxon et al., 2020), Central Europe (LamaH-CE, Klingler et al., 2021), Australia (CAMELS-AUS, Fowler et al., 2021, 2024), Switzerland (CAMELS-CH, Höge et al., 2023), Germany (CAMELS-DE, Loritz et al., 2024), India (CAMELS-INDIA, Mangukiya et al., 2024) and Denmark (CAMELS-DK, Liu et al., 2024). In recent efforts, the CAMELS have been aligned for further consistency in the CARAVAN dataset that the hydrologic community can extend via a corresponding cloud-based platform (Kratzert et al., 2023). Yet, as the forcing data of the CARAVAN dataset is extracted from the coarse ERA5 reanalysis data, a few deficiencies in the data quality, and especially the overestimated potential evaporation, need to be kept in mind when applying the dataset (Clerc-Schwarzenbach et al., 2024).

CAMELS-LUX data is available for 56 catchments, that drain into the Luxembourgish stream network at some point. Catchments in CAMELS-LUX are heterogeneous from a physiographic point of view and homogenous from a climatic perspective. The density of stations is rather high and allows a unique view of physiographic controls on rainfall-runoff transformation processes (and how they may be affected by changes in climate). The provided catchments are incorporated in a nested setup and include a few rather homogeneous, small headwater catchments. The catchments are characterized by basic geographic data such as the catchment area, the outlet location, and major water courses, as well as data on geology and land-use classes within the catchments. These classes are grouped based on their hydrologic properties. Additionally, topographic measures are included, which can assist in more accurately classifying the catchments.

Most of the catchment's time series range from 01.11.2004-31.10.2021, with a few catchments being limited by the availability of discharge observations. The time series are available at three temporal resolutions: 15 minutes, hourly, and daily. The high temporal resolution of the CAMELS-LUX dataset allows analyses of convective short-term extreme precipitation events and possible subsequent runoff events in small catchments. The time series covered in the dataset encompasses stream flow, aggregated radar precipitation (RadKlim, Winterrath et al., 2018), interpolated station precipitation (from AGE - Luxembourgish Water Agency, 2022; ASTA - Luxembourgish Ministry of Agriculture, 2024; DWD - German Weather Service, 2024; LIST - Luxembourg Institute of Science and Technology, Hydro-Climatological Observation network (HOST), 2022; MeteoLux, 2024) as well as atmospheric and soil moisture reanalysis data (ERA 5, Hersbach et al., 2023a, b; Muñoz Sabater, 2019). Rainfall is often influenced by large-scale atmospheric patterns, making atmospheric parameters a valuable source of additional information about meteorological conditions (Lengfeld et al., 2019). The atmospheric parameters of this CAMELS-LUX dataset were chosen due to their relevance during thunderstorms (Meyer et al., 2022). Consequently, they allow better identification

https://doi.org/10.5194/essd-2024-482
Preprint. Discussion started: 26 May 2025

of extreme precipitation and atmospheric conditions favouring flash floods. Among the currently available CAMELS datasets, CAMELS-LUX is the only one including atmospheric data.

2 Hydro-meteorologic time series

2.1 Discharge

Discharge data for Luxembourg was collected from stations of the Luxembourgish Water Agency (AGE) and the Luxembourg Institute of Science and Technology (LIST). The discharge data for the German region was provided by the LfU-RLP - Rhineland-Palatine State Office for Environment (2022).

Discharge is measured at 56 stream gauges that contribute to the Luxembourgish stream network. This stream network includes headwater catchments covering parts of Belgium, France, and Germany. The Our and the Sure River in the East, mark the border between Luxembourg and Germany. The original temporal resolution of the discharge measurements is 15 minutes. This time step dictates the minimum resolution for this dataset. Data were aggregated to hourly and daily time steps. For most catchments, data is available for the entire temporal interval of this dataset. Ten catchments (ID 12, 20, 31, 36, 37, 38, 46, 54, 55, 56) do not cover the entire interval of this dataset and typically start one or two years later. Significantly shorter time series are included for catchments where flash floods were observed (ID 55-56).

Discharge data was processed to interpolate all gaps in the time series. The data gaps were examined individually and compared to neighbouring stream gauges. Decisions were taken individually according to the following "rules": If the gaps only covered very few time steps, in which no precipitation fell, data was interpolated linearly. If there was rainfall and the streamflow was not in a recession period, the specific discharge was transferred from the nearest stream gauge, which reacted similarly to the one missing during the weeks around the data gap. The respective stream gauges used for filling are listed in Supplement S2. The discharge (Q [m^3/s]) was then upscaled according to the catchment area. In the dataset, a flag column was introduced to indicate interpolated values: "0" are original values, and "1" stands for linear interpolation. All further numbers are surrounding stream gauges.

2.2 Precipitation

2.2.1 Radar data

The precipitation radar data is derived from the radar product RadKlim ("Radar-based Precipitation Climatology" - YW) by the German Weather Service (DWD, version 2017.002 - Winterrath et al., 2018). RadKlim is a reprocessed and quasi gauge-adjusted version of the DWD's operational Radolan ("Radar-Online-Adjustment") product. The data quality is high, even though precipitation might be underestimated during extreme rainfall events (Kreklow et al., 2020; Pöschmann et al., 2021).

The radar data was spatially aggregated over each catchment. The 1 km × 1 km sized grid cells were considered for a catchment if their centre point lies within its area. The Weierbach (ID 50) is by far the smallest catchment within the dataset

https://doi.org/10.5194/essd-2024-482
Preprint. Discussion started: 26 May 2025

(0.46 km^2) and does not contain any radar grid cell centre. In this case, we averaged the four grid cells, that partly overlay the catchment.

The original data has a temporal resolution of 5 minutes and was accumulated to this dataset's 15-minute, hourly, and daily time step. Apart from the aggregated rain rate, we extracted the maximum and the minimum rain rate at the original 1 km^2 and 5-minute resolution. The 5-minute maximum rain rate can be used as an indicator of the precipitation intensity during an extreme event. The 15-minute, hourly, and daily resolution of the data still contains the minimum and maximum rain rate per 5 minutes within the respective time steps.

In case missing values persisted in the final time series per catchment, these gaps were eventually filled with an interpolated station data product described in the next paragraph. The 5-minute minimum and maximum rain rates in the dataset are filled with the minimum and maximum of the station data and calculated from a further disaggregation. They do not represent the maximum 5-minute rain rate and are therefore not comparable to the radar data but are the closest we could extract from the rain gauges. All values that are replaced within the radar precipitation time series are marked with a flag, that is set to 1.

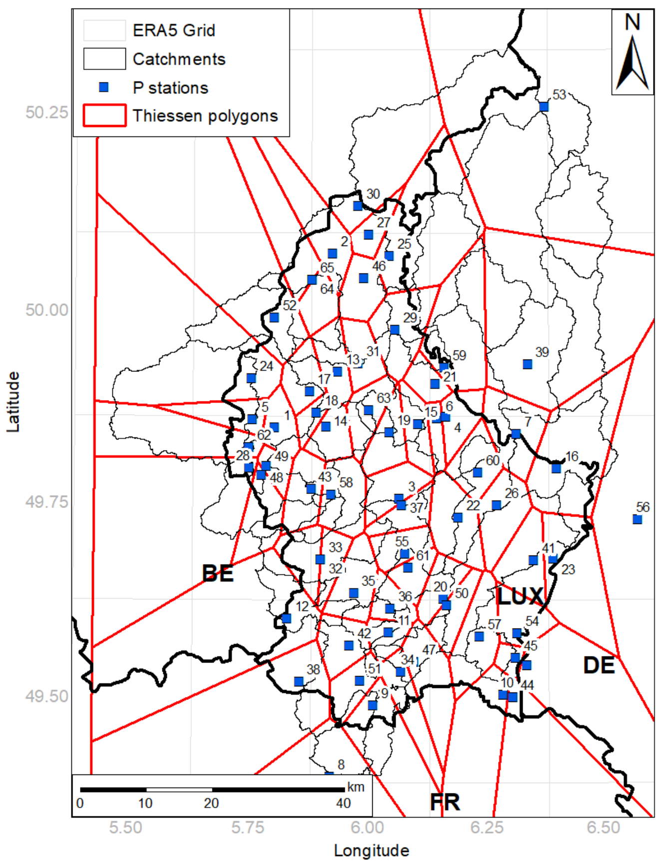

Figure 1. Precipitation stations and Thiessen polygons for the interpolation to the catchments.

https://doi.org/10.5194/essd-2024-482
Preprint. Discussion started: 26 May 2025

2.2.2 Interpolated rain gauge data

To complement the radar data, we added the spatially interpolated rain gauge data as an extra time series. We used 66 stations (listed in Supplement S1) that are spread over Luxembourg and Germany, maintained by the AGE - Luxembourgish Water Agency (2022), the ASTA - Luxembourgish Ministry of Agriculture (2024), the LIST - Luxembourg Institute of Science and Technology, Hydro-Climatological Observation network (HOST) (2022), MeteoLux (2024) or the DWD - German Weather Service (2024). This data is available at an hourly resolution for Luxembourg and a 10-minute resolution for Germany. We disaggregated or aggregated data respectively to reach the 15-minute, hourly, and daily temporal resolutions. The disaggregation for the 15-minute values should be considered when using the station data at high resolution. The gaps of each station time series were filled with data from the nearest neighbour. We then calculated Voronoi polygons (Fig. 1) to determine the weighting of each station across the catchments.

The rainfall products can differ substantially on a daily basis with maximum daily differences up to 70 mm/d (maximum daily difference radar and station data). However, the two rainfall products provided are comparable concerning the accumulated precipitation (Fig. 2 (a)). In some catchments, the radar data shows more rain, while in others, the interpolated station data does. In many cases, the sums are not distinguishable. For the strongest hourly rainfall values (Fig. 2 (b)), peak values are alternately reached by either product, showing no consistent bias. However, for medium rainfall events, the radar data consistently indicates higher precipitation amounts."

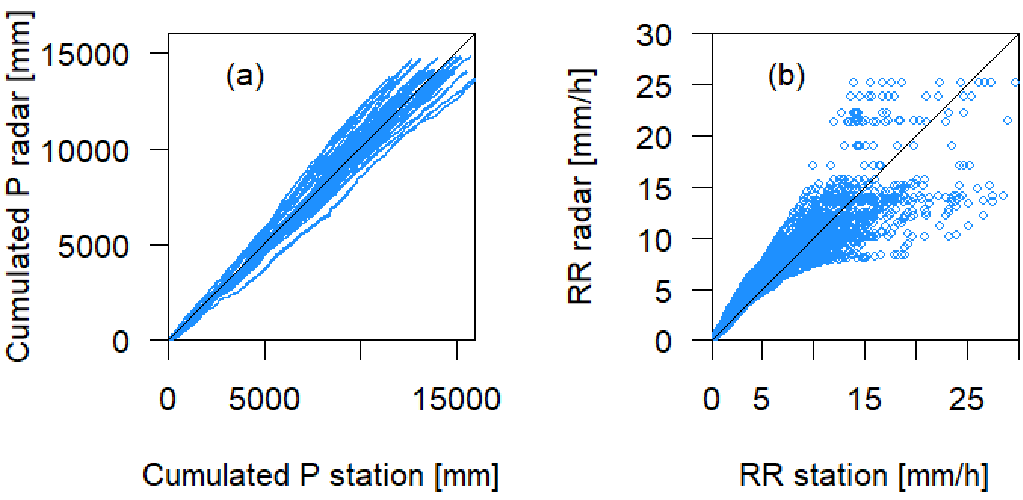

Figure 2. Comparison of the precipitation radar and station data of all catchments. Subplot (a) shows the precipitation (P) accumulated throughout the time period of this dataset (1 Nov. 2004 to 31 Oct. 2021) in all catchments. For subplot (b), the 5000 highest hourly rain rates (RR) were extracted from the two precipitation products of each catchment respectively. The rain rates were then sorted and correlated.

2.3 Potential evapotranspiration

Potential evapotranspiration (PET) (eq. 1) was computed in two ways. First, based on the air temperature (T) within the ERA5 dataset following a method by Oudin et al. (2005). R_e (MJ m^{-2} d^{-1}) is the extraterrestrial radiation, that is derived from the Julian day, the latitude, and the solar constant of approximately 0.082 MJ m^{-1}. It is divided by the latent heat flux λ (MJ kg^{-1}), that was approximated to 2.45 MJ kg^{-1}, and the density of water ρ (kg m^{-3}). The constants were set to K1=75 and K2=5. Average annual values per catchment range between 770-860 mm/yr.

$$\mathrm{PET}_{\mathrm{Oudin}} = \begin{cases} \frac{R_e}{\lambda\rho} \times \frac{(T+K_2)}{K_1} & \text{if } T + K_2 > 0 \\ 0 & \text{otherwise} \end{cases} \tag{1}$$

Secondly, we provide the PET based on the Penman-Monteith equation as shown in eq. 2 (Allen et al., 2015; Penman, 1947; Monteith, 1965). The parameters are also extracted from the ERA5 dataset and encompass R_n (net radiation), G (soil heat flux), ρ (mean air density [kg m^3]), $e_s - e_a$ (vapour pressure deficit, kPa), c_p (specific heat of dry air, 1.013 x 10^{-3}MJ kg^{-1}°C^{-1}), λ (latent heat of vaporization 2.45 MJ kg^{-1}), Δ (slope of the saturation vapour pressure temperature relationship), γ (psychrometric constant), r_s (surface resistance, m s^{-1}) and r_a (aerodynamic resistance, m s^{-1}). The PET estimated based on Penman-Monteith is around 150 mm/year higher than the PET calculated with the approach by Oudin et al. (2005) ranging from 870-1100 mm/yr. Moreover, the daily variations are substantially higher compared to the PET based on Oudin et al. (2005).

$$PET_{PM} = \frac{\Delta \cdot (R_n - G) + \rho \cdot c_p \cdot \frac{e_s - e_a}{r_a}}{\lambda \cdot \left(\Delta + \gamma \cdot \left(1 + \frac{r_s}{r_a}\right)\right)} \tag{2}$$

2.4 Atmospheric data

The ERA5 reanalysis data was downloaded from the Copernicus Climate Data Store (CDS). We extracted parameters of atmospheric data at single levels (Hersbach et al., 2023b) as well as at different pressure levels (Hersbach et al., 2023a). The specific parameters are listed in Table 1 and represent different aspects of thunderstorm formation, such as high atmospheric instability and a high moisture content. In addition, wind speeds and shear winds should be low, to allow a slow storm motion and good organisation so that a large amount of rainfall accumulates over a specific area. These atmospheric conditions favour extreme precipitation and, potentially, flash floods (Meyer et al., 2022).

The spatial resolution of the atmospheric ERA5 grid cells is 0.25° × 0.25°. To extract values over the catchments we averaged the grid cell values within each catchment, weighted by the area of each cell within the catchment. A few small catchments are located within one ERA5 grid cell only (catchments: 10, 12, 13, 16, 17, 23, 36, 53, 54, 56).

The original temporal resolution of the ERA5 data is hourly. To disaggregate the data to the 15-minute interval of the observed discharge data of our dataset, we used linear interpolation for most parameters. The values at the full hour are the

https://doi.org/10.5194/essd-2024-482
Preprint. Discussion started: 26 May 2025

Table 1. Selected proxy parameters for the assessment of convection-relevant atmospheric conditions and soil moisture data from the ERA5 dataset (adapted from Meyer et al., 2022).

Proxy for	Parameter	Abbr.	Unit	Level	Source
Instability	Convective available potential energy	CAPE	$J\,kg^{-1}$	Single	Hersbach et al. (2023b)
	Convective inhibition	CIN	$J\,kg^{-1}$	Single	Hersbach et al. (2023b)
	K index	K index	°C	Single	Hersbach et al. (2023b)
Moisture	Total column water vapour	TCWV	$kg\,m^{-2}$	Single	Hersbach et al. (2023b)
	Specific humidity	q	$kg\,kg^{-1}$	700 hPa	Hersbach et al. (2023a)
	Relative humidity	RH	%	700 hPa	Hersbach et al. (2023a)
Storm motion and organization	$\boldsymbol{u}$ component of wind	$\boldsymbol{u}$	$m\,s^{-1}$	10 m, 500 hPa and 700 hPa	Hersbach et al. (2023a)
	$\boldsymbol{v}$ component of wind	$\boldsymbol{v}$	$m\,s^{-1}$		Hersbach et al. (2023a)
Catchment wetness state	Volumetric soil water layer 1	Swvl1	$m^3\,m^{-3}$	0–7 cm	Muñoz Sabater (2019)
	Volumetric soil water layer 2	Swvl2	$m^3\,m^{-3}$	7–28 cm	Muñoz Sabater (2019)
	Volumetric soil water layer 3	Swvl3	$m^3\,m^{-3}$	28–100 cm	Muñoz Sabater (2019)
	Volumetric soil water layer 4	Swvl4	$m^3\,m^{-3}$	100–289 cm	Muñoz Sabater (2019)

original values. As the total precipitation is an accumulated value, we equally divided the hourly values for this parameter. From the original parameters, we calculated the mean wind speed ($WS_{10\,m\,a.g.l.-500\,hPa}$, eq. 3) between 10 m a.g.l. and the pressure level of 500 hPa from the squared northward direction wind vector u (m s^{-1}) and the squared eastward direction wind vector v (m s^{-1}).

$$WS_{10\,m\,a.g.l.-500\,hPa} = \sqrt{\frac{\left(u^2_{10\,m\,a.g.l.} + v^2_{10\,m\,a.g.l.}\right) + \left(u^2_{500\,hPa} + v^2_{500\,hPa}\right)}{2}} \tag{3}$$

Low-level wind shear (LLS, m s^{-1}) and deep-layer wind shear (DLS, m s^{-1}) were computed likewise to the wind speed. Yet, for the LLS (eq. 4), the difference of the vectors u and v was calculated between the near ground level and 850 hPa height (approximately 1.5 km) and for the DLS (eq. 5) respectively, the difference between near ground level and 500 hPa height (approximately 6 km).

$$LLS = \sqrt{(u_{1000\,hPa} - u_{850\,hPa})^2 + (v_{1000\,hPa} - v_{850\,hPa})^2} \tag{4}$$

$$DLS = \sqrt{(u_{1000\,hPa} - u_{500\,hPa})^2 + (v_{1000\,hPa} - v_{500\,hPa})^2} \tag{5}$$

https://doi.org/10.5194/essd-2024-482
Preprint. Discussion started: 26 May 2025

Open Access Earth System Science Data Discussions

2.5 Soil moisture

Soil moisture time series are provided for the assessment of (pre-event) wetness states of the catchments, potentially affecting infiltration capacities and subsurface flow components. Soil moisture was extracted from the ERA5 land data, which is available at a spatial resolution of 0.1° × 0.1° (Muñoz Sabater, 2019). The data was clipped to the catchments and weighted averages were built to be incorporated into the time series. The original hourly data were respectively linearly disaggregated to the 15-minute time step and aggregated to the daily time step. The soil moisture (volumetric soil water) is provided at four different levels (0-7 cm, 7-28 cm, 28-100 cm, 100-289 cm) as indicated in Table 1.

3 Physiographical setting of Luxembourg

3.1 Regional context

Luxembourg lies in central-western Europe, bordering France, Belgium, and Germany (Fig. 5). The country is characterized by two geographic regions with largely differing characteristics: The Oesling region in the North and the Gutland region in the South of the country. The Oesling forms a part of the Ardennes massif, with a schistose and steep bedrock geology. The area hosts only a few settlements and a substantial forested part. In contrast, the Gutland region, which is the northeastern tip of the Paris Basin, features soft valleys in sedimentary rocks that form the basis for extensive agriculture and urban areas. In the East of Luxembourg, the Mosel valley marks the border with Germany. The valley offers milder climatic conditions perfectly suited for viticulture.

3.2 Climate

The relatively homogeneous climate of Luxembourg is characterized by westerly atmospheric circulation coming from the Atlantic (Pfister et al., 2000) and classified as a temperate oceanic climate (Kottek et al., 2006). The mean annual rainfall is 700-900 mm (this dataset (2003-2020), Pfister et al., 2005, (1971-2000)) and spreads almost equally throughout the year (Fig. 3), with around 100 mm/month during the winter and 70 mm/month in the late summer (Wrede et al., 2015). The mean monthly temperatures (1971-2000) vary seasonally from about 0°C in January to 18°C in July (Pfister et al., 2005). The potential evapotranspiration (PET) calculated using the Oudin et al. (2005) method, based on air temperature, and the Penman-Monteith equation ranges from 800 to 1000 mm per year (Fig. 3). The Mosel Valley area is prone to heavy thunderstorms between May and August, with relatively regular daily precipitation values above 100 mm (Schmithüsen, 1940). Within the last 20 years (2001-2020), a slight increase in thunderstorm favouring conditions was observed throughout the entire country (Meyer et al., 2022).

3.3 Hydrology

The hydrological regime within Luxembourg is pluvial oceanic (Pardé, 1947), characterized by humid catchments (aridity indices > 1, Fig. 3 h). Streamflow regimes are characterized by high water levels and flooding during the winter and low flows

https://doi.org/10.5194/essd-2024-482
Preprint. Discussion started: 26 May 2025

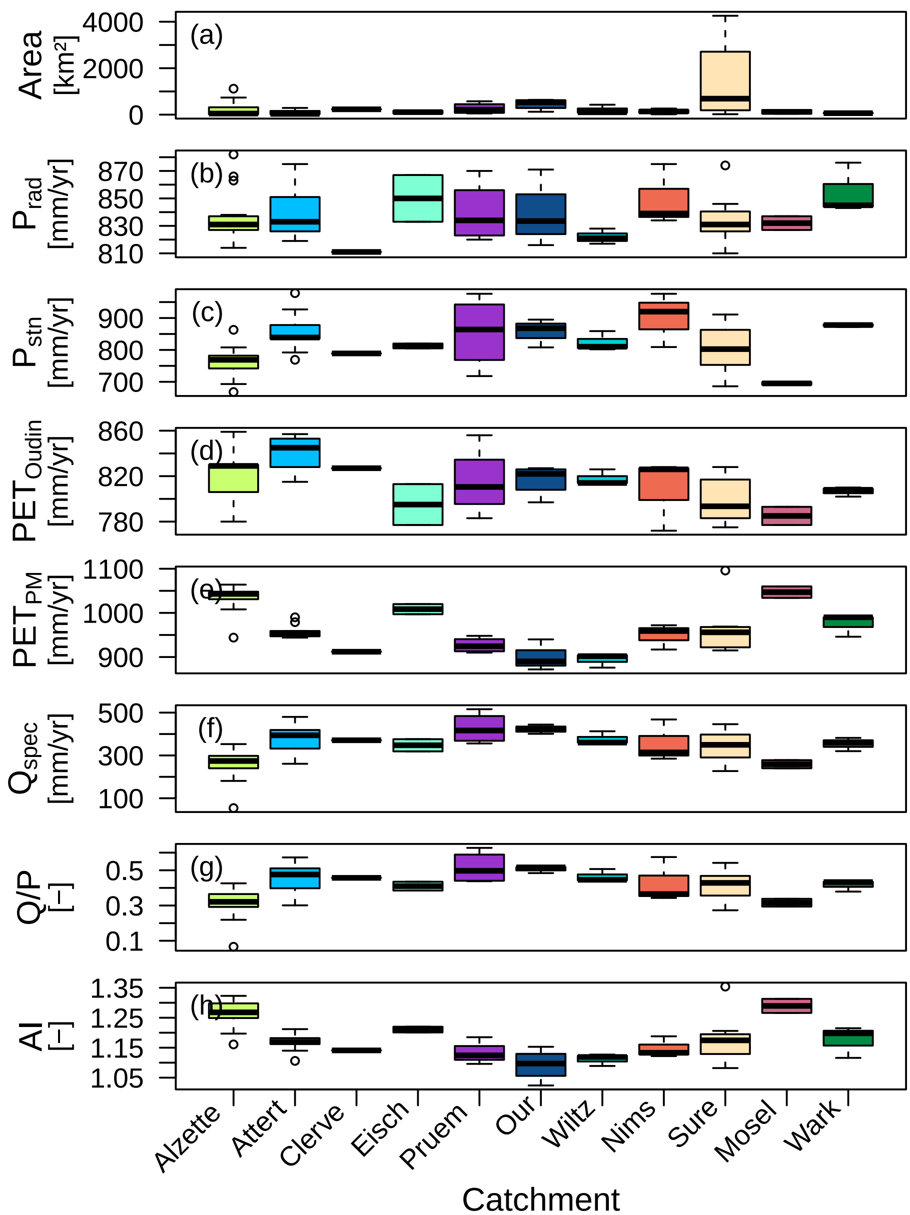

Figure 3. Water balance related catchment variables per major river basins. Subplot (a) indicates the range of the catchment sizes, (b) and (c) show the annual rainfall based on the radar product and respectively the station interpolation, (d) and (e) show the annual potential evapotranspiration calculated according to Oudin et al. (2005) and Penman-Monteith, (f) shows the specific discharge, (g) shows the derived annual runoff ratio (Q/P) and the aridity index is shown in subplot (h).

https://doi.org/10.5194/essd-2024-482
Preprint. Discussion started: 26 May 2025

during the summer (Wrede et al., 2015). Runoff ratios (Q/P) range between 0.3 and 0.5 (Fig. 3 g). While from 1980 to 2000 large winter floods were observed on multiple occasions (Pfister et al., 2000), they have been observed less frequently within the last 20 years. Floods triggered by thunderstorms at the beginning of summer have been increasingly observed between 2016 and 2021 (Bingenheimer, 2018; Pfister et al., 2018).

Luxembourg contains a nested system of headwater catchments contributing to a few rivers of a higher order (Fig. 4). These are the Attert and Wark in the West, the Alzette in the South, and the Wiltz, Clerve, and Our in the North of the country. East of the latter three on the German side are the Pruem and Nims catchments. All of these contribute to the Sure River, that feeds the Mosel at Trier, East of Luxembourg. The Syre and Aalbach rivers in the East of Luxembourg flow directly into the Mosel. Widespread thunderstorms on 22 July 2016 (Pfister et al., 2018) and 01 June 2018 (Pfister et al., 2020), caused flash floods within the White Ernz and Aalbach catchments, and significant runoff in many of the other catchments in the database. Another severe flooding event directly following heavy rainfall hit Luxembourg and surrounding regions in Belgium and Germany in mid-July 2021. While the rainfall triggered flash floods in Germany, the Luxembourgish streams had slower rising water levels (e.g., Kreienkamp et al., 2021). Large-scale floods during the winter occurred - among others - in the first week of January 2010 and in January 2020.

3.4 Geology

Luxembourg is divided in two major natural regions, consisting of distinct geological and geomorphological features (Fig. 5 b). The northern region (called ’Oesling’) covers nearly one third of the country and is a part of the Ardennes-Rhenish shield. In the southern region (called ’Gutland’) Mesozoic sediments prevail and form the northeastern limit of the Paris Basin.

In the Oesling, the limited permeability of the schistous bedrock causes surface and lateral subsurface flows to dominate streamflow generation. The Gutland region is characterized by alternating layers of permeable (e.g., sandstone) and less permeable (e.g., marls) bedrock layers. The former allows a deep percolation of water towards large aquifers that eventually feed a constant baseflow component in the river network (Gourdol et al., 2024; Wrede et al., 2015). In catchments dominated by substrates with limited permeability, fast hydrological processes - such as saturation excess overland flow - dominate streamflow generation (Wrede et al., 2015). Based on geological data from Luxembourg (APC - Administration des ponts et chaussées, 2022), Belgium (Hellebrand et al., 2007), France (BRGM - Bureau de Recherches Géologiques et Minière, 2020) and Germany (BGR - Bundesanstalt für Geowissenschaften und Rohstoffe, 2019), five geology classes were determined, based on their hydrological behaviour and featured permeability (Pfister et al., 2017): (1) marl and claystone, (2) schists & quartzites, (3) surface deposits, (4) Limestone & dolomites, (5) sandstone & conglomerates.

3.5 Land use

The North of the country is widely covered by forests and cultivated land. The South has some forested areas but is dominated by agriculture and urban areas. The hillsides towards the Mosel Valley in the East of the country are traditionally used as vineyards. Based on CORINE data (EEA - European Environment Agency, 2018) for Germany, France and Belgium and additional from Luxembourg (MECB - Ministère de l’Environnement, du Climat et du Développement durable & MEA - Ministère de

https://doi.org/10.5194/essd-2024-482
Preprint. Discussion started: 26 May 2025

Open Access Earth System Science Data Discussions

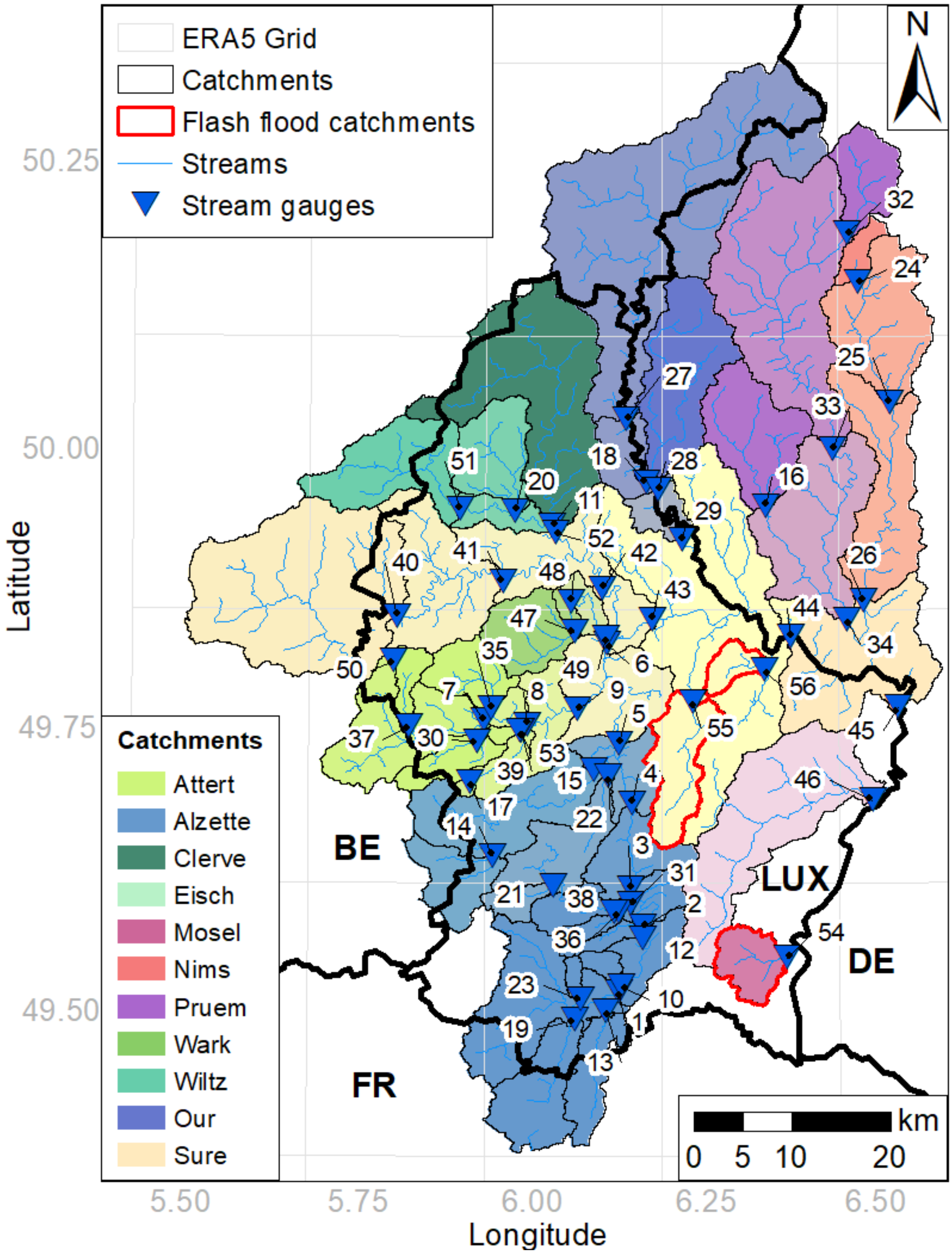

Figure 4. The 56 nested catchments of CAMELS-LUX are grouped into a few basins of higher order that are indicated by the underlying colour code. Most basins feed the Sure River (yellow), that eventually drains into the Mosel at steam gauge 45. The two south-eastern catchments (46 and 54) directly feed the Mosel. The catchments bordered in read mark the ones, in which flash floods have occurred.

https://doi.org/10.5194/essd-2024-482
Preprint. Discussion started: 26 May 2025

Open Access Earth System Science Data Discussions

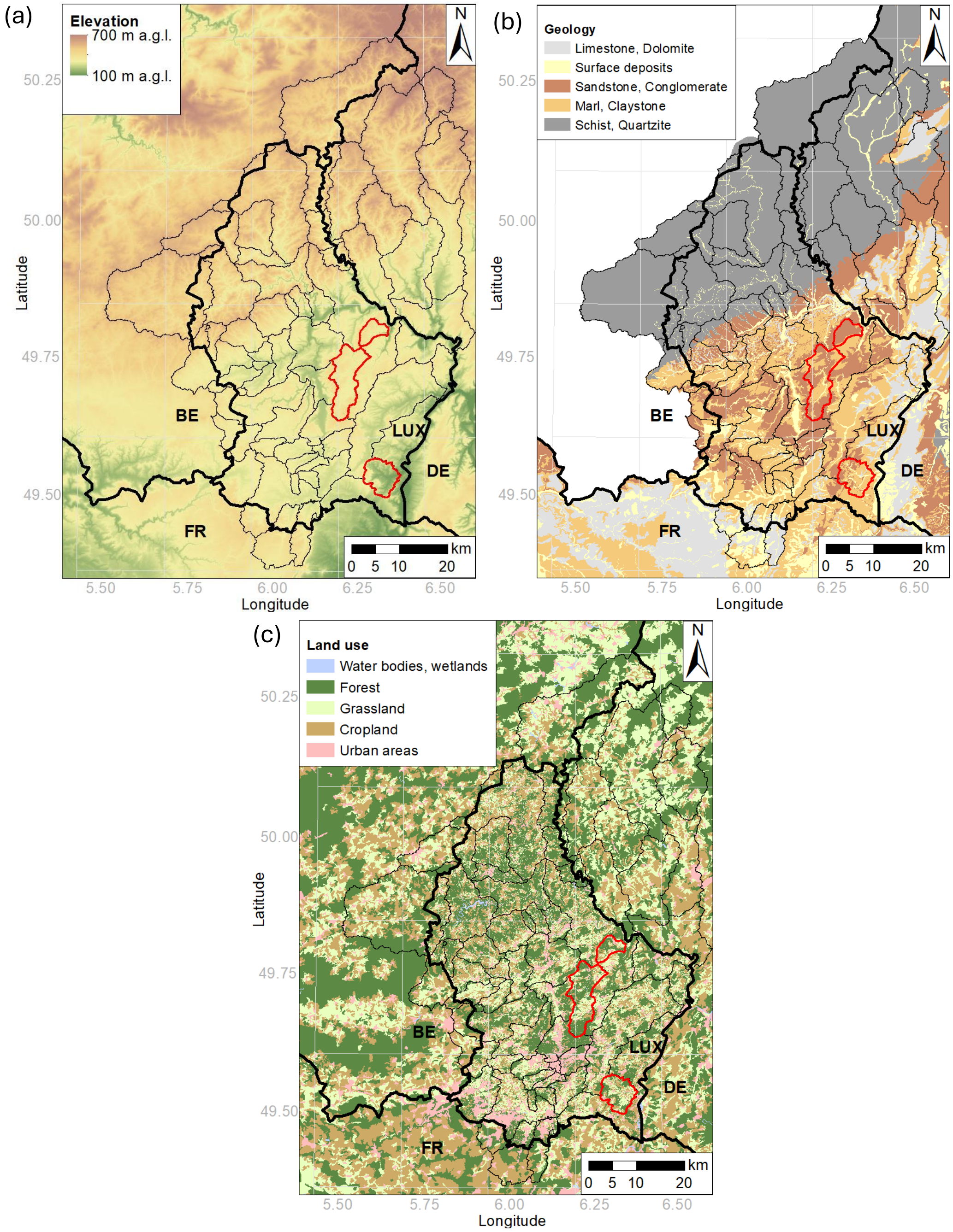

Figure 5. Physiographic settings of the catchments in and around Luxembourg. Subplot (a) illustrates the topography. Subplot (b) shows the underlying geology that is grouped into five classes based on their hydrological behaviour. Subplot (c) shows the distribution of the five determined land use classes.

https://doi.org/10.5194/essd-2024-482
Preprint. Discussion started: 26 May 2025

l'énergie et de l'Aménagement du territoire, 2018) land use was grouped into five classes: water bodies & wetlands, forests & natural areas, grassland, agricultural land, and urban areas (Fig. 5 c).

4 Topography and derived morphometric parameters

The topography of Luxembourg is shown in Fig. 5 (a). The North of Luxembourg, the Oesling region, is a mountainous region, that is a part of the Ardennes massif that extends from France to Germany. In Belgium, the Ardennes massif reaches elevations of up to 600-700 m a.s.l. (Pfister, 2012). In Luxembourg, the highest peak is reached in Wilwerdange with an elevation of 560 m a.s.l. Valleys are cut in deep V-shapes. The South of the country, the Gutland area, lies at the eastern limit of the Paris basin (Wrede et al., 2015) and ranges from approximately 100-400 m a.s.l.. Hills are softer and the landscape and U-shaped valleys are wider. The South-Eastern border of Luxembourg is defined by the Mosel valley, which cuts deeply into the surrounding hills. An area of the central East of Luxembourg, the Mullerthal, is characterized by steep and rocky slopes.

A 5 x 5 m digital elevation model (DEM) was constructed for the entire study area based on data from Luxembourg (ACT - Administration du Cadastre et de la Topographie, 2019), Belgium (SPW - Service Public de Wallonie, 2014), France (IGN - Institut National de l'Information Géographique et Forestière: RGE ALTI, 2020), North Rhine-Westphalia (IT-NRW - Information und Technik Nordrhein-Westfalen, 2021), Rhineland-Palatinate (LVG - Landesamt für Vermessung und Geobasisinformation, 2021) and (Hengl et al., 2022). The catchments of the 56 stream gauges have been extracted from this DEM, using the hydrological network to ensure consistency. In addition to basic catchment characteristics (elevation, area, perimeter, and slope), a few morphometric indices relevant to the hydrologic response are described in subsections hereafter.

4.1 Gravelius compactness coefficient (K_c)

As the basin shape influences the accumulation of runoff, and therefore the hydrographs of flood peaks, the Gravelius compactness coefficient (K_c) was included in the hydrologic catchment properties. Its calculation is based on the ratio of the basin's perimeter and the perimeter of a circle of the catchment's area (eq. 6). K_c values close to 1 indicate a circular catchment shape. The roundest catchment of this dataset is the Weierbach (ID 50) with K_c = 1.133. The larger K_c values are, the more elongated a catchment is (Gravelius, 1914). In this dataset, the highest K_c = 2.202 is calculated in the Sure catchment at Bollendorf (ID 44).

$$K_c = \frac{\text{Perimeter}}{2\sqrt{\pi \times \text{Area}}} \tag{6}$$

4.2 Network Development and Persistence Index (IDPR)

The river Network Development and Persistence Index (IDPR) was incorporated into the dataset as an assessment tool for infiltration capacities of the soil or ground. It can be considered a proxy for the catchment's drainage density making it an indicator for both topographic and hydrological catchment properties (Mardhel et al., 2021; Uhan et al., 2004). The IDPR quantifies the discrepancy between the observed natural river system and a theoretical hydrographic network calculated only

https://doi.org/10.5194/essd-2024-482
Preprint. Discussion started: 26 May 2025

from a DEM for a given accumulation threshold (set to 62.5 hectares in this study). The IDPR is the ratio of the shortest distance following the steepest slope of a point considered to (a) the theoretical river system and (b) the actual river system. Originally this ratio was arbitrarily multiplied by 1000 and limited to a maximum value of 2000 (Mardhel et al., 2021). A transformation of this ratio into a logarithmic value (base 10) was preferred in this study (eq. 7). Negative values indicate areas prone to infiltration, while positive values indicate areas that favour surface runoff. The IDPR is often in agreement with the fraction of a priori impermeable geologic formations in the basin. The range of the catchments´ mean IDPR in this dataset reaches from -0.501 (Kaylbach, ID 19, mainly limestone and dolomites) to 0.615 (Weierbach, ID 50, schist).

$$\text{IDPR} = log\frac{a}{b} \tag{7}$$

4.3 Topographic wetness index (TWI)

The Topographic Wetness Index (TWI) was developed by Beven and Kirkby (1979) and describes the spatial variation of soil moisture within a catchment. Its calculation (eq. 8) is based on the upstream contributory area (topographic area drained at the point considered) (α) and the local surface slope in radian (β). TWI values provide information about the ability of a point to accumulate water as a function of the amount of water flowing in and escaping from it. An area with high TWI values is characterized by an increased potential for accumulated runoff and therefore a higher probability of getting saturated. On the other hand, sectors with steep slopes and close to ridgelines will have a TWI close to zero. In this dataset, TWI catchment means range from 5.846 (Huewelerbach, ID 17) to 7.146 (Eisch, ID 14).

$$\text{TWI} = \ln\left(\frac{\alpha}{\tan\beta}\right) \tag{8}$$

4.4 Vector Ruggedness Measure (VRM)

Terrain roughness is characterized in this dataset by the Vector Ruggedness Measure (VRM) index. It measures the dispersion in three dimensions of orthogonal vectors on the terrain surface (x, y, z) and thus incorporates variability in both the aspect (β) and the slope (α). Proposed by Hobson (1972) and adapted by Sappington et al. (2007), the VRM index is dimensionless and ranges from 0 to 1. Typical values for natural soils vary between 0 and 0.5. Rugged landscapes are defined by values greater than 0.01-0.02. Here, mean VRM values at the catchment scale range from 0.001 (Wollefsbach, ID 53) to 0.011 (Enz, ID 16).

$$\text{VRM} = 1 - \frac{|r|}{n} \tag{9}$$

with

$$|r| = \sqrt{\left(\sum x\right)^2 + \left(\sum y\right)^2 + \left(\sum z\right)^2} \quad (10)$$

$$z = 1 \times \cos(\alpha) \quad (11)$$

$$xy = 1 \times \sin(\alpha) \quad (12)$$

$$x = xy \times \sin(\beta) \quad (13)$$

$$y = xy \times \cos(\beta) \quad (14)$$

(15)

5 Catchment behaviour

Luxembourg's nested catchment setup is ideally suited for studying the influence of the underlying bedrock on fundamental hydrological functions of water collection, storage, mixing, and release. While the climate is relatively constant throughout the study area, the geology is highly contrasted. Bedrock geology controls both the rainfall-runoff transformation and catchment storage properties, as revealed by several studies based on a subset of 16 Luxembourgish catchments (Pfister et al., 2017; Wrede et al., 2015). The dominant geological bedrock categories found in Luxembourg are represented by small and relatively homogeneous experimental headwater catchments: the Wollefsbach (ID 53) dominated by marly bedrock, the schistose Weierbach (ID 50), and the sandstone-dominated Huewelerbach (ID 17) (Wrede et al., 2015). Catchments dominated by marly substrate tend to react fast to precipitation inputs and their runoff regime is highly seasonal (with very pronounced low flows in summer, in comparison to high winter discharge). Due to the very limited permeability of marls, lateral subsurface flow dominates the rainfall-runoff transformation and preferential pathways often contribute to flashy responses. Depending on soil water content, saturation excess overland flow may equally trigger fast and important flood events. On schist bedrock, catchments also exhibit a strongly seasonal rainfall-runoff behaviour and subsurface lateral flow rather frequently observed. Typically fast runoff reactions are caused by overland flow near saturated riverine areas and fast subsurface flow through macropores. Slower runoff reactions are proper to phases with higher soil humidity and groundwater levels. During winter, the combination of these two (fast and slow) processes cause the Weierbach's typical double peak pattern (Hissler et al., 2021; Martínez-Carreras et al., 2016). The permeable sandstone formations allow deep percolation and hold large storage capacities that feed the streams with a nearly constant baseflow throughout the year (Wrede et al., 2015).

In Fig. 6, we provide a conceptualisation of the meaning of the morphologic parameters in comparison to the geology classes in which the catchments were grouped. As suggested through the topographic wetness index (Fig. 6 a), catchments with a high percentage of marl and claystone have a higher TWI than catchments that are dominated by schist and quartzite or sandstone and conglomerate. Designed to assess infiltration capacities, the IDPR increases with less bedrock permeability and decreases with higher bedrock permeability (Fig. 6 d). When considering catchment geomorphology (Fig. 6 e), softer geological structures exhibit flatter (U-shaped) slopes, compared to the steep (V-shaped) slopes proper to schist geology. This is coherent with the lower surface roughness in areas dominated by marls, in comparison to schist areas (Fig. 6 g). Additionally,

https://doi.org/10.5194/essd-2024-482
Preprint. Discussion started: 26 May 2025

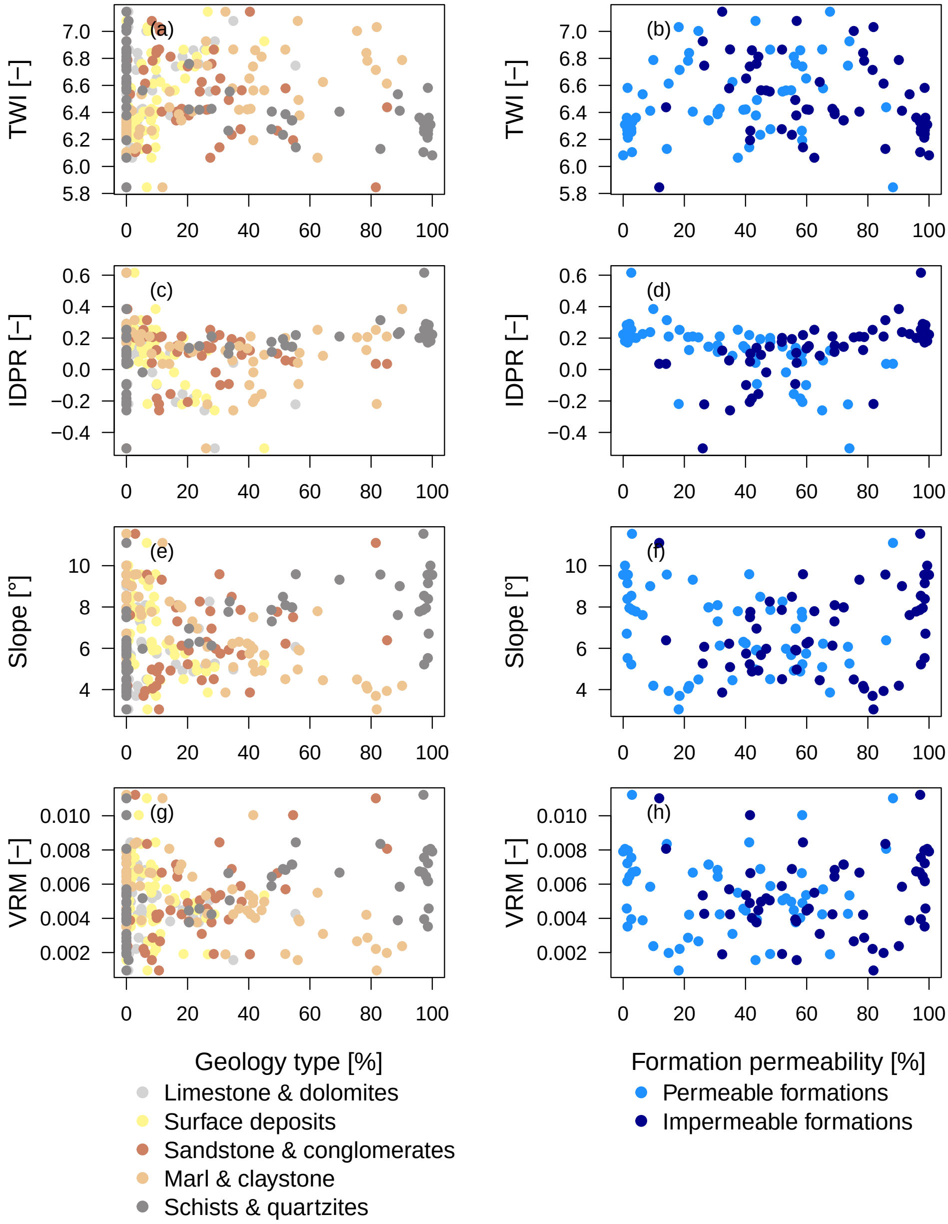

Figure 6. Morphologic parameters in correlation to the catchments' percentage of certain geology types. The left column refers to the percentage of all geology classes themselves and in the right column, the geology is grouped into permeable and impermeable formations. Subplots (a)-(b) show the Topographic Wetness Index (TWI), subplots (c)-(d) the river Network Development and Persistence Index (IDPR), subplots (e)-(f) the catchments' slope and the subplots (g)-(h) the Vector Ruggedness Measure (VRM).

land use patterns are influenced by both topography and geology. In schistose areas, forests cover steep hills, while agricultural

https://doi.org/10.5194/essd-2024-482
Preprint. Discussion started: 26 May 2025

activities are mostly located on the plateaus. Contrarily, in the South of Luxembourg, agriculture is mostly concentrated in the marly valleys and forests are limited to the sandstone plateaus.

We would like to highlight the peculiar hydrological behaviour of a few catchments. Due to its very permeable sandstone bedrock, the Huewelerbach (ID 17) has an exceptionally high storage capacity, leading to substantial volumes of water percolating into deep groundwater bodies. At the interface between permeable sandstone and less permeable marls, springs provide a continued and very stable baseflow contribution to the Huewelerbach. The Kaylbach (ID 19) and the Dudelingerbach (ID 13) have been strongly influenced by mining activities in the past. Baseflow continues to be sustained by pumping of water infiltrated in flooded mining galleries. The catchments react to strong summer rainfall events, essentially generated by rapid surface and subsurface flows. The Pétrusse (ID 31) catchment is a telling example of rainfall-runoff responses from urbanized catchments. The City of Luxembourg covers approximately one-third of the catchment, contributing to a flashy response to intense rainfall events (leading occasionally to so-called first-flush pollution events). The Weierbach (ID 50) is characterized by natural double peak flow hydrographs during high storage levels of the catchment.

6 Data set application

6.1 Atmospheric parameters characterizing thunderstorms

Atmospheric parameters have been included to better describe thunderstorms. This allows us to analyze the 2016 and 2018 flash floods and their potential increase due to climate change. The atmospheric parameters in this dataset have been chosen as proxies for atmospheric conditions that have the potential for the development of rain-intense thunderstorms. The parameters can be classified into three groups, that can be considered the ingredients for thunderstorm development: high atmospheric moisture, sufficient atmospheric instability, and slow wind speeds to keep the system motion low and allow the system to dump all its rain over one area. This combination can potentially trigger flash floods. The long-term trends (1981-2020) of these parameters were studied in Meyer et al. (2022). Significantly increasing trends were found in the proxies for an abundant atmospheric moisture content (specific humidity, q, and total column water vapour, TCVW). Yet, relative humidity decreased slightly. These results follow the Clausius-Clapeyron relation, showing that higher air temperatures allow for increased absolute water content in the air. However, in terms of relative humidity, this increase is leveled out. Moreover, the proxy parameters representing instability (convective available potential energy (CAPE) and the K index) have increased between 1981 and 2020. Yet, convective inhibition (CIN) has increased, which controls the gains in CAPE (Taszarek et al., 2021). Parameters referring to the system motion and organization have remained unchanged. Trends were especially strong within the second half of the period, from 2001 to 2020. This corresponds approximately to the interval of this dataset (2004-2021). This dataset is used to set up a regional model for Luxembourg. Including atmospheric data in the modelling process will allow identifying atmospheric conditions that favour thunderstorms. This can give additional information to the model to describe flood generation, even when the triggering precipitation is not accurately represented. The regional catchment analysis also allows for the inclusion of catchments with limited data. This is the case of catchments where flash floods occurred in 2016 and 2018, which are of particular interest.

https://doi.org/10.5194/essd-2024-482
Preprint. Discussion started: 26 May 2025

6.2 Benchmark model LSTM

6.2.1 Model setup and training

To provide a reference for model intercomparison studies, a benchmark Long-Short-Term-Memory (LSTM) model for Luxembourg was added to this dataset. This benchmark model utilizes all dynamic time series and a selection of physiographic catchment characteristics as input features (Appendix E). The LSTM hyperparameters were selected based on literature references (e.g. Acuña Espinoza et al., 2024). For the daily data, a sequence length of 365 days was chosen to reflect the annual hydrological cycle. The model includes one LSTM layer that is coupled with a linear head layer, both with a hidden size of 64. It was trained to optimize the area-averaged Nash-Sutcliffe efficiency (Kratzert et al., 2019b) over 30 epochs with a batch size of 256, with a dropout rate of 40% and an initial learning rate of 0.001. The learning rate was adjusted by a gamma rate of 0.8 every five epochs. The forget gate was initially set to a value of 3. In the presented simulations based on CAMELS-LUX, three differing training periods were compared. Training in the first half of the dataset (shown in Fig. 7 a) is compared to training on the second half of the dataset (Fig. 7 b). This distinction was made as all observed flash floods were observed in the second half of this dataset's time period. Thirdly, (Fig. 7 c), a training period in the middle of the time period was chosen to include one series of flash floods (2016) in the training and test on the second one (2018). More details about the LSTM are described in Acuña Espinoza et al. (2024). For an overview of how LSTMs function in hydrology, please refer to Kratzert et al. (2019a).

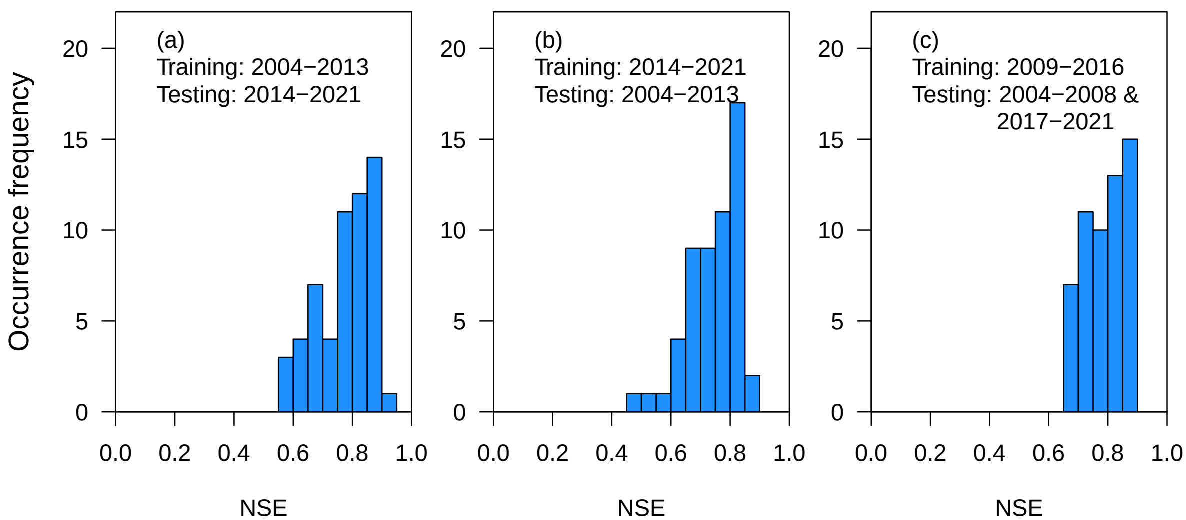

Figure 7. NSE distribution of the 56 catchments during three different model runs with varying testing and training periods. Subplot (a) was trained on data from 2004-2013 and tested on data from 2014-2021. Subplot (b), respectively on the inverted periods. As flash floods were observed only in the second half of this dataset's time period, a third training period in the middle was chosen. Subplot (c) shows simulations trained on data from 2009-2016 and tested on the time periods before and after that. This training period from 2009 to 2016 includes the first observed series of flash floods in 2016.

https://doi.org/10.5194/essd-2024-482
Preprint. Discussion started: 26 May 2025

6.2.2 General evaluation of the LSTM performance

With these hyperparameter settings, the model achieved efficiencies in the test periods with a Nash-Sutcliffe Efficiency (NSE) ranging from 0.4 to 0.9, varying based on the choice of testing and training periods as well as different training runs (see Fig. 7). Fig. 8 shows the spatial distribution of the NSE values. One catchment that is particularly challenging to simulate with this LSTM, as well as other hydrological models (Wrede et al., 2015), is the Huewelerbach (ID 17), which is presumed to lose groundwater to deep percolation in a sandstone aquifer. Similarly, the Kaylbach (ID 19) is difficult to simulate due to the groundwater´s infiltration into mining galleries. The weak performance is related to a non-closing water balance that has also been found in highly conductive chalk or karstic aquifers in Great Britain and Southern Texas and might - among others - also be related to insufficiently characterizing catchment attributes (Lees et al., 2021; Feng et al., 2020). The White Ernz (ID 55) and Hallerbach (ID 56) have significantly shorter periods of available data and are not always well-represented in model training, which also explains their low performance scores. The overall performance of this model is however reasonably good and compares to the results of other studies based on CAMELS datasets (e.g., Gauch et al., 2021; Acuña Espinoza et al., 2024; Lees et al., 2021).

6.2.3 Evaluation in dependence of the static catchment characteristics

Larger catchments reach NSE values at the upper end of the range, while there is a wide spread of NSE values in smaller catchments (0-100 km^2) (Fig. 9 a, b). The NSE is higher in catchments with a higher elevation range and a higher mean slope (Fig. 9 d, e). The second row of Fig. 9 (f-j) shows the model performances across the five geology classes, while the third row (k-o) shows performance across land use classes. Given the wide range of NSE values, we conclude that the performance of the LSTMs is not dependent on either geology or land use.

However, the evaluation of the model based on catchment characteristics is likely influenced by correlations between geology, elevation, and land use. The catchments in the North of Luxembourg lie in the schistose Ardennes mountain range, where steep valleys have formed and forests dominate vast parts of the plateau. The South of Luxembourg is characterized by alternating sandstone and marl, which form large valleys at a generally lower elevation. The major land use type is related to agriculture and urban areas. As storage-controlled floods during winter are simulated more precisely than summer peak flows, we had anticipated, that catchments with large storage capacities (i.e. sandstone) would be easier to simulate for the LSTM model than catchments with higher surface runoff components and flashier character. This is however not the case.

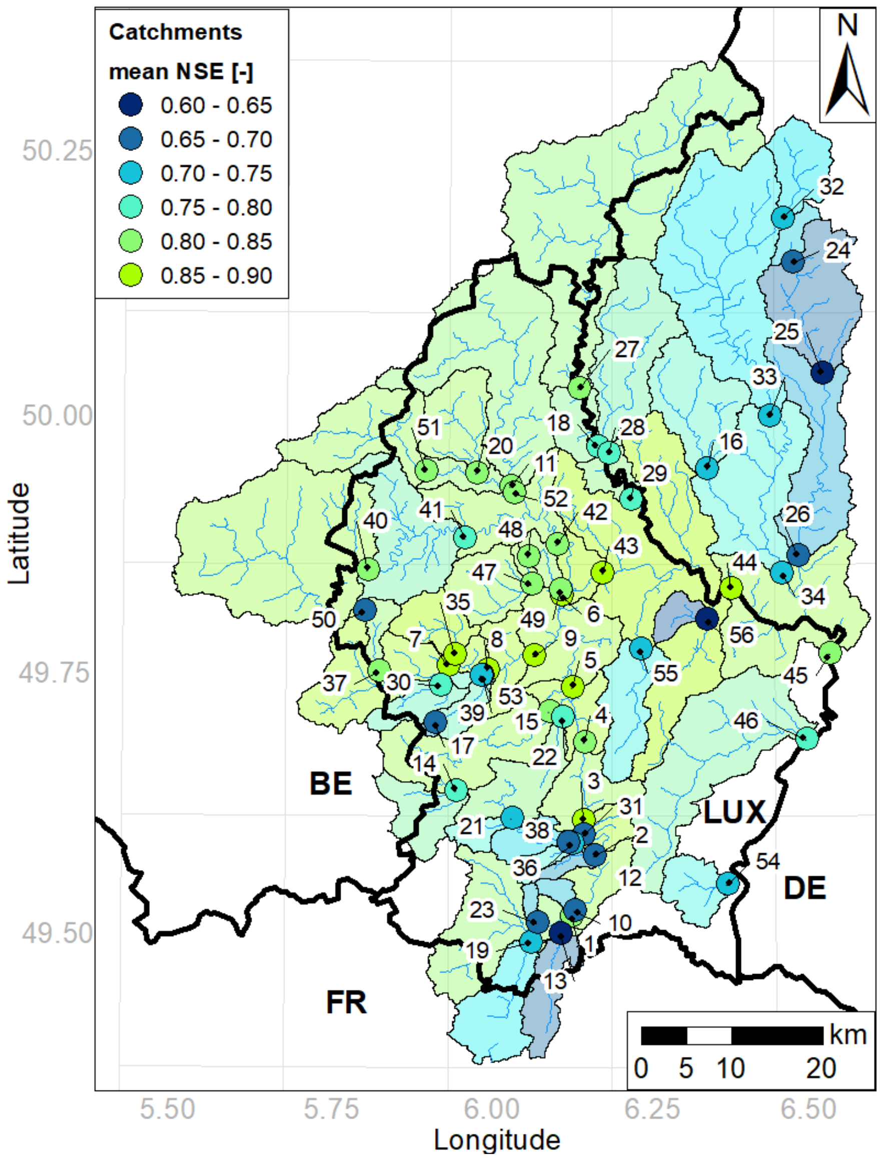

Figure 8. The map shows the Nash-Sutcliffe Efficiency (NSE) of the model performance in each catchment respectively. The green colour code indicates the best performances, the dark blue colour the worst. Please be aware of the nested catchment setup that leads to some overlapping of the results. The NSE displayed is based on the mean of the three model runs with differing testing periods that were described above.

.

https://doi.org/10.5194/essd-2024-482
Preprint. Discussion started: 26 May 2025

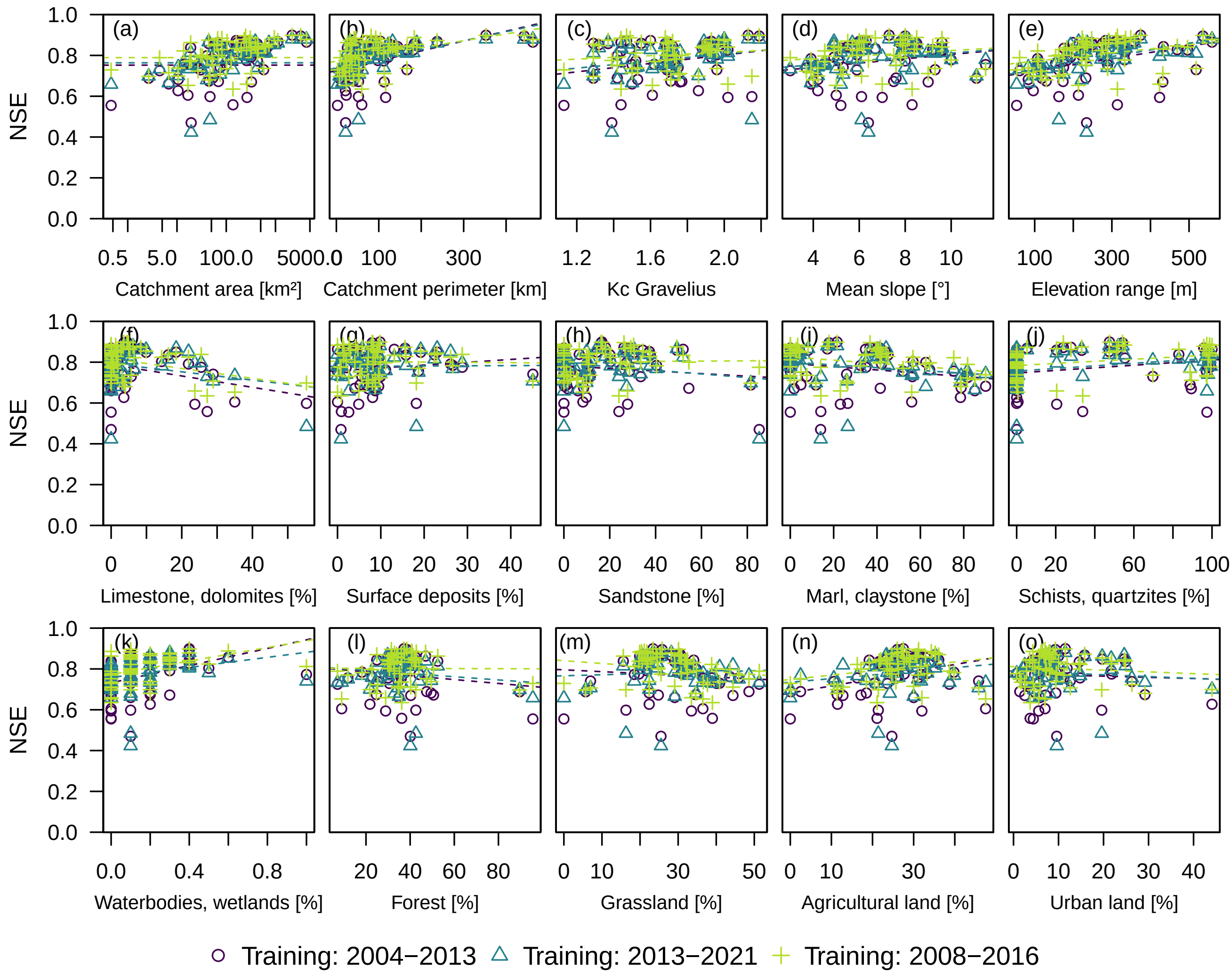

Figure 9. Links between the general model performance as evaluated by the Nash-Sutcliffe Efficiency (NSE) and differing static catchment characteristics. Note the logarithmic horizontal axis in subplot (a). The subplots (a)-(c) include catchment metadata, such as area, perimeter, and shape, (d) and (e) address topographic properties. The second row (f)-(j) displays the effect of a catchment's differing percentage of the five geology classes, while the third row (k)-(o) refers to the five land use classes. The three differing symbols relate to the three model runs based on different training periods.

.

https://doi.org/10.5194/essd-2024-482
Preprint. Discussion started: 26 May 2025

Open Access Earth System Science Data Discussions

7 Conclusions

375 The presented CAMELS-LUX dataset describes a comprehensive inventory of hydro-meteorological and atmospheric data for Luxembourg and its surrounding areas. CAMELS-LUX was compiled from data from different Luxembourgish and German agencies and institutes. All 56 presented catchments are classified by geological, land use, and topographic features that allow extensive regional analyses.

The data is available at three different temporal resolutions. In addition to the daily data, which is the general time step 380 of other CAMELS datasets (e.g., Addor et al., 2017; Coxon et al., 2020; Loritz et al., 2024), we provide the time series in an hourly and 15-minute time step . This subdaily resolution allows studying faster runoff processes following thunderstorms and potentially flash floods, where flood waves usually develop within only a few hours (Marchi et al., 2010). Capturing the temporal dimension of these hillslope processes, channel routing and network geomorphology proves especially crucial in small catchments, where they dominate the temporal hydrologic response of a catchment (Robinson et al., 1995). The 385 presented nested catchment setup of CAMELS-LUX contains many of the small scale catchments. Moreover, most applied flood forecasting models are using an hourly or even higher temporal resolution. In ongoing work, we are further testing the benefits of the higher resolution in the regional modelling approach.

Based on CAMELS-LUX, we succeeded in setting up and training a regional model for Luxembourg and can conclude that the LSTM can simulate discharge across catchments with varying physiographic settings in and around Luxembourg. It is the 390 first time that simulations have been made in many of the small catchments achieving reasonable results (NSE ranging between 0.4 and 0.9). This already shows that the dataset can lead to a better understanding of the large-scale hydrology in the Greater Region of Luxembourg. The presented benchmark model could be beneficial for filling data gaps and forecasting applications and leaves room for further optimization.

Appendix A: Dataset properties

Table A1. Global dataset properties at a glimpse.

Catchments:	56
Time period:	Most catchments 1 Nov. 2004 to 31 Oct. 2021
Time zone:	UTC +1
Temporal resolutions:	3 versions: 15 minutes, 1 hour, 1 day

https://doi.org/10.5194/essd-2024-482
Preprint. Discussion started: 26 May 2025

Appendix B: List of catchments

Table B1. 56 nested catchments within the CAMELS-LUX dataset listed with their meta data.

ID	Gauge (Stream)	Lat	Lon	Area [km^2]	Start	End
1	Livange (Alzette)	49.526477	6.114957	258.34	2004	2021
2	Hesperange (Alzette)	49.586287	6.14908	317.78	2004	2021
3	Pfaffenthal (Alzette)	49.620647	6.132266	388.96	2004	2021
4	Hunsdorf (Alzette)	49.69895	6.13361	441.91	2004	2021
5	Mersch (Alzette)	49.753068	6.115991	736.86	2004	2021
6	Ettelbruck (Alzette)	49.8448	6.098584	1118.33	2004	2021
7	Reichlange (Attert)	49.774226	5.925732	159.49	2004	2021
8	Useldange (Attert)	49.770335	5.985998	247.50	2004	2021
9	Bissen(Attert)	49.784853	6.056414	289.29	2004	2021
10	Livange (Bibeschbach)	49.531667	6.119773	10.63	2004	2021
11	Kautenbach (Clerve)	49.952417	6.021154	230.91	2004	2021
12	Hesperange (Drosbech)	49.586287	6.14908	10.51	2006	2021
13	Bettembourg (Dudelingerbach)	49.508908	6.097123	46.87	2004	2021
14	Hagen (Eisch)	49.650346	5.937105	50.96	2004	2021
15	Hunnebour (Eisch)	49.729184	6.079524	167.00	2004	2021
16	Sinspelt (Enz)	49.970411	6.322601	101.43	2004	2021
17	Huewelerbach (Huewelerbach)	49.71825	5.905708	2.66	2004	2021
18	Gemund (Irsen)	49.992541	6.154194	125.35	2004	2021
19	Kayl (Kaylbach)	49.500286	6.052986	75.21	2004	2021
20	Merkholtz (Kirel)	49.965897	5.968539	66.88	2006	2021
21	Mamer (Mamer)	49.623206	6.023054	17.93	2004	2021
22	Schoenfels (Mamer)	49.723112	6.100795	81.65	2004	2021
23	Huncherange (Mierbech)	49.518907	6.061947	6.80	2004	2021
24	Giesdorf (Nims)	50.174633	6.454355	16.69	2004	2021
25	Seffern (Nims)	50.064356	6.499988	137.10	2004	2021
26	Alsdorf-Oberecken (Nims)	49.883608	6.462262	264.21	2004	2021
27	Dasbourg (Our)	50.049832	6.126077	447.93	2004	2021
28	Gemund (Our)	49.985333	6.1715	612.05	2004	2021
29	Vianden (Our)	49.939224	6.204738	636.88	2004	2021
30	Niederpallen (Pall)	49.754673	5.91413	32.97	2004	2021

https://doi.org/10.5194/essd-2024-482
Preprint. Discussion started: 26 May 2025

Table B2. Long table continued.

ID	Gauge (Stream)	Lat	Lon	Area [km^2]	Start	End
31	Luxembourg (Petrusse)	49.606702	6.132359	44.58	2004	2020
32	Prüm (Prüm)	50.21939	6.439864	53.12	2004	2021
33	Echtershausen (Prüm)	50.022304	6.418312	325.58	2004	2021
34	Prümzurlay (Prüm)	49.866647	6.437269	575.71	2004	2021
35	Platen (Roudbach)	49.785259	5.935675	43.96	2004	2021
36	Cessange (Ruisseau de Cessange)	49.598469	6.12	13.6904	2007	2021
37	Colpach (Rau de Colpach)	49.768578	5.819138	18.96	2006	2021
38	Merl (Ruisseau de Merl)	49.59941	6.109055	26.78	2005	2021
39	Useldange (Schwebich)	49.76472	5.977705	30.13	2004	2021
40	Bigonville (Sure)	49.869821	5.801399	308.35	2004	2021
41	Heiderscheidergrund (Sure)	49.901196	5.950724	429.91	2004	2021
42	Michelau (Sure)	49.895421	6.091178	946.48	2004	2021
43	Diekirch (Sure)	49.866622	6.161813	2176.73	2004	2021
44	Bollendorf (Sure)	49.850919	6.359193	3243.51	2004	2021
45	Rosport (Sure)	49.785883	6.509851	4256.62	2004	2021
46	Mertert (Syre)	49.701803	6.4738	201.64	2005	2021
47	Niederfeulen (Wark)	49.855534	6.052637	57.39	2004	2021
48	Welscheid (Wark)	49.883032	6.047939	64.33	2004	2021
49	Ettelbruck (Wark)	49.850643	6.09738	81.35	2004	2017
50	Weierbach (Weierbach)	49.828415	5.797152	0.46	2004	2021
51	Winseler (Wiltz)	49.967894	5.890266	103.87	2004	2021
52	Kautenbach (Wiltz)	49.946524	6.025045	427.94	2004	2021
53	Useldange (Wollefsbach)	49.764402	5.975416	4.49	2004	2021
54	Bous (Aalbach)	49.557468	6.352567	40.86	2006	2021
55	Larochette (Ernz Blanche)	49.791584	6.219358	69.31	2015	2021
56	Hallerbach (Hallerbach)	49.820722	6.321401	19.40	2006	2016

https://doi.org/10.5194/essd-2024-482
Preprint. Discussion started: 26 May 2025

Open Access Earth System Science Data Discussions

Appendix C: Time series in the dataset

Table C1. Time series in the dataset.

Proxy for	Parameter	Abbr.	Unit	Level	Source
Hydrology	Discharge	Q	m^3/s	Gauge	AGE, LIST, LFU
	Specific discharge	Qspec	mm	Gauge	calculated
	Flag for Q	Q_flag	-	-	determined
Precipitation	Rain rate (radar)	RR_rad	mm	Radar	Winterrath et al. (2018), gaps filled with station data by ASTA, AGE, LIST, DWD
	Min. rain rate (radar)	RR_min_rad	mm/5Min/1x1km	Radar	
	Max. rain rate (radar)	RR_max_rad	mm/5Min/1x1km	Radar	
	Flag for P	RR_flag_rad	-	-	
	Rain rate (Station)	RR_stn	mm	Station	AGE, LIST, ASTA, DWD
	Rain rate (ERA5)	tp	mm	single	Hersbach et al. (2023b)
Temperature	Air temperature	t2m	°C	single, 2m	Hersbach et al. (2023b)
Water balance	Potential evapotranspiration	PET_Oudin	mm		Calc. according to Oudin et al. (2005)
	Potential evapotranspiration	PET_PM	mm		Calc. according to Penman-Monteith Allen et al. (2015)
Instability	Convective available potential energy	CAPE	$J\ kg^{-1}$	single	Hersbach et al. (2023b)
	Convective inhibition	CIN	$J\ kg^{-1}$	single	Hersbach et al. (2023b)
	K-Index	Kx	°C	single	Hersbach et al. (2023b)
Moisture	Total column water vapour	TCWV	$kg\ m^{-2}$	single	Hersbach et al. (2023b)
	Specific humidity	q	$kg\ kg^{-1}$	700 hPa	Hersbach et al. (2023a)
	Relative humidity	RH	%	700 hPa	Hersbach et al. (2023a)
Storm motion and organisation	Wind speed	WS	$m\ s^{-1}$	10 m & 500 hPa	Calc. from Hersbach et al. (2023a)
	Low-level wind shear	LLS	$m\ s^{-1}$	10 m & 850 hPa	
	Deep-layer wind shear	DLS	$m\ s^{-1}$	10 m & 500 hPa	
Catchment wetness state	Volumetric soil water layer 1	Swvl1	$m^3\ m^{-3}$	0-7 cm	Muñoz Sabater (2019)
	Volumetric soil water layer 2	Swvl2	$m^3\ m^{-3}$	7-28 cm	Muñoz Sabater (2019)
	Volumetric soil water layer 3	Swvl3	$m^3\ m^{-3}$	28-100 cm	Muñoz Sabater (2019)
	Volumetric soil water layer 4	Swvl4	$m^3\ m^{-3}$	100-289 cm	Muñoz Sabater (2019)

https://doi.org/10.5194/essd-2024-482
Preprint. Discussion started: 26 May 2025

Open Access Earth System Science Data Discussions

Appendix D: Static climatological and physiographic catchment characteristics

Table D1. Static climatological and physiographic catchment characteristics. The climatic and hydrologic values are calculated based on the hourly data of the dataset.

Proxy for	Parameter	Abbr.	Unit	Source
General	Discharge system	catchment		
	X	XLuref		LUREF (EPSG:2169)
	Y	YLuref		LUREF (EPSG:2169)
	Latitude	Lat	°	WGS84 (EPSG:4326)
	Longitude	Lon	°	WGS84 (EPSG:4326)
	Area	area_km2	km^2	
	Perimeter	perimeter_km	km	
	Gravelius compactness coefficient	Kc_Gravelius	-	Calculated according to Gravelius (1914)
Climate & Hydrology	Total annual specific discharge	Qspec_sum	mm	[2003-2020] LfU-RLP - Rhineland-Palatine State Office for Environment (2022); AGE - Luxembourgish Water Agency (2022); LIST - Luxembourg Institute of Science and Technology, Hydro-Climatological Observation network (HOST) (2022)
	Mean annual air temp.	t2m_mean	°C	ERA5, Hersbach et al. (2023b)
	Min. hourly air temp.	t2m_min	°C	ERA5, Hersbach et al. (2023b)
	Max. hourly air temp.	t2m_max	°C	ERA5, Hersbach et al. (2023b)
	Total annual precip. (radar)	prad_sum	mm	Winterrath et al. (2018)
	Total annual precip. (stations)	pstn_sum	mm	AGE - Luxembourgish Water Agency (2022); LIST - Luxembourg Institute of Science and Technology, Hydro-Climatological Observation network (HOST) (2022); ASTA - Luxembourgish Ministry of Agriculture (2024); DWD - German Weather Service (2024)
	Total annual potential evapotranspiration	PET_Oudin_sum	mm	Calculated according to Oudin et al. (2005)
	Total annual potential evapotranspiration	PET_PM_sum	mm	Calculated according to Penman-Monteith (Allen et al., 2015)
	Aridity Index	AI_Oudin	-	(PET_Oudin/rr_rad)
	Aridity Index	AI_PM	-	(PET_PM/rr_rad)
	Mean annual runoff ratio	runoffratio	-	(Q/rr_rad)

https://doi.org/10.5194/essd-2024-482
Preprint. Discussion started: 26 May 2025

Table D2. Long table continued.

Proxy for	Parameter	Abbr.	Unit	Source
Geology	Limestone & dolomites		%	BGR - Bundesanstalt für Geowissenschaften und Rohstoffe (2019)
	Surface deposits		%	APC - Administration des ponts et chaussées (2022)
	Sandstone & conglomerates		%	BRGM - Bureau de Recherches Géologiques et Minière (2020)
	Marl & claystone		%	Hellebrand et al. (2007)
	Schists & quartzites		%	
	Permeable formations		%	
	Impermeable formations		%	
Land use	Watercourses & waterbodies & wetlands		%	Based on EEA - European Environment Agency (2018)
	Forests & natural areas		%	MECB - Ministère de l'Environnement, du Climat et du Développement durable & MEA - Ministère de l'énergie et de l'Aménagement du territoire (2018)
	Grassland		%	
	Cropland		%	
	Urban areas		%	
Topography	Elevation	Z	m.a.s.l.	ACT - Administration du Cadastre et de la Topographie (2019) Hengl et al. (2022) IT-NRW - Information und Technik Nordrhein-Westfalen (2021) IGN - Institut National de l'Information Géographique et Forestière: RGE ALTI (2020) LVG - Landesamt für Vermessung und Geobasisinformation (2021) SPW - Service Public de Wallonie (2014)
	Network Development and Persistence Index	IDPR	-	Calculated according to Mardhel et al. (2021)
	Slope	Slope	°	
	Topographic wetness index	TWI	-	Beven and Kirkby (1979)
	Vector roughness measure	VRM	-	Sappington et al. (2007)

https://doi.org/10.5194/essd-2024-482
Preprint. Discussion started: 26 May 2025

Appendix E: Benchmark model settings - LSTM-LUX

Table E1. LSTM model settings: Time series, static catchments attributes and hyperparameters.

	Abbr.	
Dynamic time series	Qflag, RR_rad, RR_min_rad, RR_max_rad, RR_flag_rad, RR_stn, tp, t2m, PET_Oudin, cape, cin, kx, q, rh, tcwv, ws10500, lls, dls, swvl1, swvl2, swvl3, swvl4	
Static catchment attributes	Area_km2, Kc_Gravelius, limestone_dolomites, surface_deposits, sandstone_conglomerates, marl_claystone, schists_quarzites, watercourses_waterbodies_wetlands, forests_naturalareas_grassland_agricultural_land, urban, Z_RANGE, IDPR_MEAN, SLOPE_MAX, TWI_MEAN, VRM_MEAN	
Hyperparameters	Time step	daily
	No. of layers	1
	Sequence length	365
	Hidden size	64
	Batch size	265
	No. of epochs	30
	Drop out rate	0.4
	Learning rate	0.001
	Adapt learning rate epoch	5
	Gamma adapt learning rate	0.8
	Forget gate	3

https://doi.org/10.5194/essd-2024-482
Preprint. Discussion started: 26 May 2025

Open Access Earth System Science Data Discussions

Data availability

The CAMELS-LUX dataset is available on zenodo: https://doi.org/10.5281/zenodo.13846619, where we have moreover enclosed a detailed data description (Nijzink et al., 2024).

Author contributions. JN collected and processed the hydro-meteorologic time series data and wrote the first draft. DZ calculated the PET following Penman-Monteith and tested the dataset. LG calculated the topographic indices for the catchment characterization. RL provided the model code for the benchmark model. All the co-authors (JN, LG, JFI, RL, DZ and LP) contributed to and edited the manuscript.

Competing interests. The authors declare that they have no conflict of interest.

Acknowledgements. We acknowledge all of the providers of data used in this work: the German Weather Service (DWD) for the RadKlim radar data; the Luxembourgish Water Agency (AGE), the Luxembourgish Ministry of Agriculture (ASTA), the Luxembourgish weather service (MeteoLux), the Luxembourg Institute and Science and Technology (LIST) and the German Weather Service (DWD), for the precipitation station data; the Copernicus Climate Change Service for the ERA5 dataset; and the Luxembourg Institute and Science and Technology (LIST) and the Luxembourgish Water Agency (AGE) for the discharge data. This research has been supported by the Fonds National de la Recherche Luxembourg (FNR) (grant no. PRIDE15/10623093/HYDRO-CSI).

Supplement

S1 List of precipitation stations

S2 List of stream gauges used for interpolations of discharge data

https://doi.org/10.5194/essd-2024-482
Preprint. Discussion started: 26 May 2025

References

ACT - Administration du Cadastre et de la Topographie: LiDAR 2019 - Modèle numérique de terrain (MNT), https://data.public.lu/fr/datasets/lidar-2019-modele-numerique-de-terrain-mnt/, accessed: 2024-05-25, 2019.

Acuña Espinoza, E., Loritz, R., Álvarez Chaves, M., Bäuerle, N., and Ehret, U.: To bucket or not to bucket? Analyzing the performance and interpretability of hybrid hydrological models with dynamic parameterization, Hydrology and Earth System Sciences, 28, 2024.

Addor, N., Newman, A. J., Mizukami, N., and Clark, M. P.: The CAMELS data set: Catchment attributes and meteorology for large-sample studies, Hydrology and Earth System Sciences, 21, 5293–5313, https://doi.org/10.5194/hess-21-5293-2017, 2017.

AGE - Luxembourgish Water Agency: Hourly Precipitation, 15-minute Discharge, accessed: 2022-04-01, 2022.

Allen, R. G., Pereira, L. S., Raes, D., and Smith, M.: Crop Evapotranspiration - Guidelines for computing crop water requirements, https://www.researchgate.net/publication/235704197, 2015.

Alvarez-Garreton, C., Mendoza, P. A., Boisier, J. P., Addor, N., Galleguillos, M., Zambrano-Bigiarini, M., Lara, A., Puelma, C., Cortes, G., Garreaud, R., McPhee, J., and Ayala, A.: The CAMELS-CL dataset: Catchment attributes and meteorology for large sample studies-Chile dataset, Hydrology and Earth System Sciences, 22, 5817–5846, https://doi.org/10.5194/hess-22-5817-2018, 2018.

APC - Administration des ponts et chaussées: Carte géologique harmonisée, https://geocatalogue.geoportail.lu/geonetwork/srv/fre/catalog.search#/metadata/542a0caa-4b33-4019-8ce7-b8541b436106, accessed: 2024-05-25, 2022.

ASTA - Luxembourgish Ministry of Agriculture: AgriMeteo: Precipitation data, https://www.agrimeteo.lu/Agrarmeteorologie/Wetterdaten/Niederschlag, accessed: 2024-06-23, 2024.

Beven, K. J. and Kirkby, M. J.: A physically based, variable contributing area model of basin hydrology, Hydrological Sciences Bulletin, 24, 43–69, https://doi.org/10.1080/02626667909491834, 1979.

BGR - Bundesanstalt für Geowissenschaften und Rohstoffe: Geoportal der Bundesanstalt für Geowissenschaften und Rohstoffe, https://produktcenter.bgr.de/terraCatalog/DetailResult.do?fileIdentifier=0f2e1b5b-fc02-4491-a12b-2178473f5c84, accessed: 2024-05-25, 2019.

Bingenheimer, V.: Starkregen bringt Überschwemmungen im Zentrum und im Osten, Luxemburger Wort, https://www.wort.lu/luxemburg/starkregen-bringt-ueberschwemmungen-im-zentrum-und-im-osten/945939.html, accessed: 2024-07-06, 2018.

BRGM - Bureau de Recherches Géologiques et Minière: Téléchargement des cartes géologiques départementales à 1/50 000 (Bd Charm-50), https://infoterre.brgm.fr/formulaire/telechargement-cartes-geologiques-departementales-150-000-bd-charm-50, accessed: 2024-05-25, 2020.

Chagas, V. B., Chaffe, P. L. B., Addor, N., Fan, F. M., Fleischmann, A. S., Paiva, R. C. D., and Siqueira, V. A.: CAMELS-BR: Hydrometeorological time series and landscape attributes for 897 catchments in Brazil, Earth System Science Data, 12, 2075–2096, https://doi.org/10.5194/essd-12-2075-2020, 2020.

Clerc-Schwarzenbach, F. M., Selleri, G., Neri, M., Toth, E., van Meerveld, I., and Seibert, J.: HESS Opinions: A few camels or a whole caravan?, EGUsphere [preprint], pp. 1–29, https://doi.org/10.5194/egusphere-2024-864, 2024.

Coxon, G., Addor, N., Bloomfield, J. P., Freer, J., Fry, M., Hannaford, J., Howden, N. J., Lane, R., Lewis, M., Robinson, E. L., Wagener, T., and Woods, R.: CAMELS-GB: hydrometeorological time series and landscape attributes for 671 catchments in Great Britain, Earth System Science Data, 12, 2459–2483, https://doi.org/10.5194/essd-12-2459-2020, 2020.

DWD - German Weather Service: Open data: 10-minute precipitation data, https://opendata.dwd.de/climate_environment/CDC/observations_germany/climate/10_minutes/precipitation/historical/, accessed: 2024-06-23, 2024.

EEA - European Environment Agency: CORINE Land Cover 2018 (vector/raster 100 m), Europe, 6-yearly, Version 2020-2021, https://doi.org/10.2909/960998c1-1870-4e82-8051-6485205ebbac, accessed: 2024-05-25, 2018.

Feng, D., Fang, K., and Shen, C.: Enhancing Streamflow Forecast and Extracting Insights Using Long-Short Term Memory Networks With Data Integration at Continental Scales, Water Resources Reseach, 56, https://doi.org/10.1029/2019WR026793, 2020.

Fowler, K. J., Acharya, S. C., Addor, N., Chou, C., and Peel, M. C.: CAMELS-AUS: Hydrometeorological time series and landscape attributes for 222 catchments in Australia, Earth System Science Data, 13, 3847–3867, https://doi.org/10.5194/essd-13-3847-2021, 2021.

Fowler, K. J. A., Zhang, Z., and Hou, X.: CAMELS-AUS v2: updated hydrometeorological timeseries and landscape attributes for an enlarged set of catchments in Australia, Earth System Science Data Discussions, 2024, 1–21, https://doi.org/10.5194/essd-2024-263, 2024.

Gauch, M., Kratzert, F., Klotz, D., Nearing, G., Lin, J., and Hochreiter, S.: Rainfall-runoff prediction at multiple timescales with a single Long Short-Term Memory network, Hydrology and Earth System Sciences, 25, 2045–2062, https://doi.org/10.5194/hess-25-2045-2021, 2021.

Gourdol, L., Stewart, M. K., Morgenstern, U., and Pfister, L.: Short high-accuracy tritium data time series for assessing groundwater mean transit times in the vadose and saturated zones of the Luxembourg Sandstone aquifer, Hydrology and Earth System Sciences, 28, 3519–3547, https://doi.org/10.5194/hess-28-3519-2024, 2024.

Gravelius, H.: Flusskunde 1, vol. 1, Göschen, potamology edn., 1914.

Hellebrand, H., Hoffmann, L., Juilleret, J., and Pfister, L.: Hydrology and Earth System Sciences Assessing winter storm flow generation by means of permeability of the lithology and dominating runoff production processes, Hydrol. Earth Syst. Sci, 11, 1673–1682, https://doi.org/10.5194/hess-11-1673-2007, 2007.

Hengl, T., Parente, L. L., Krizan, J., and Bonannella, C.: Continental Europe Digital Terrain Model at 30 m resolution based on GEDI, ICESat-2, AW3D, GLO-30, EUDEM, MERIT DEM and Background Layers. Distributed by OpenTopography, https://doi.org/10.5281/zenodo.4724549, accessed: 2024-05-25, 2022.

Hersbach, H., Bell, B., Berrisford, P., Biavati, G., Horányi, A., Muñoz Sabater, J., Nicolas, J., Peubey, C., Radu, R., Rozum, I., Schepers, D., Simmons, A., Soci, C., Dee, D., and Thépaut, J.-N.: ERA5 hourly data on pressure levels from 1940 to present, Copernicus Climate Change Service (C3S) Climate Data Store (CDS), https://doi.org/10.24381/cds.bd0915c6, 2023a.

Hersbach, H., Bell, B., Berrisford, P., Biavati, G., Horányi, A., Sabater, J. M., Nicolas, J., Peubey, C., Radu, R., Rozum, I., Schepers, D., Simmons, A., Soci, C., Dee, D., and Thépaut, J.-N.: ERA5 hourly data on single levels from 1940 to present, Copernicus Climate Change Service (C3S) Climate Data Store (CDS), https://doi.org/10.24381/cds.adbb2d47, 2023b.

Hissler, C., Martínez-Carreras, N., Barnich, F., Gourdol, L., Iffly, J. F., Juilleret, J., Klaus, J., and Pfister, L.: The Weierbach experimental catchment in Luxembourg: A decade of critical zone monitoring in a temperate forest - from hydrological investigations to ecohydrological perspectives, Hydrological Processes, 35, https://doi.org/10.1002/hyp.14140, 2021.

Hobson, R. D.: Surface roughness in topography: quantitative approach, in: Spatial analysis in geomorphology, edited by Chorley, R. J., pp. 221–245, Harper and Row, New York, 1972.

Höge, M., Kauzlaric, M., Siber, R., Schönenberger, U., Horton, P., Schwanbeck, J., Floriancic, M. G., Viviroli, D., Wilhelm, S., Sikorska-Senoner, A. E., Addor, N., Brunner, M., Pool, S., Zappa, M., and Fenicia, F.: CAMELS-CH: hydro-meteorological time series and landscape attributes for 331 catchments in hydrologic Switzerland, Earth System Science Data, 15, 5755–5784, https://doi.org/10.5194/essd-15-5755-2023, 2023.

IGN - Institut National de l'Information Géographique et Forestière: RGE ALTI: Le modèle numérique de terrain (MNT) maillé qui décrit le relief du territoire français à grande échelle, https://geoservices.ign.fr/rgealti, accessed: 2024-05-25, 2020.

https://doi.org/10.5194/essd-2024-482
Preprint. Discussion started: 26 May 2025

IT-NRW - Information und Technik Nordrhein-Westfalen: Digitales Geländemodell - Gitterweite 1 m - Paketierung: Einzelkacheln, https://www.opengeodata.nrw.de/produkte/geobasis/hm/dgm1_xyz/dgm1_xyz/, accessed: 2024-05-25, 2021.

Klingler, C., Schulz, K., and Herrnegger, M.: LamaH-CE: LArge-SaMple DAta for Hydrology and Environmental Sciences for Central Europe, Earth System Science Data, 13, 4529–4565, https://doi.org/10.5194/essd-13-4529-2021, 2021.

Kottek, M., Grieser, J., Beck, C., Rudolf, B., and Rubel, F.: World map of the Köppen-Geiger climate classification updated, Meteorologische Zeitschrift, 15, 259–263, https://doi.org/10.1127/0941-2948/2006/0130, 2006.

Kratzert, F., Klotz, D., Herrnegger, M., Sampson, A. K., Hochreiter, S., and Nearing, G. S.: Toward Improved Predictions in Ungauged Basins: Exploiting the Power of Machine Learning, Water Resources Research, 55, 11 344–11 354, https://doi.org/10.1029/2019WR026065, 2019a.

Kratzert, F., Klotz, D., Shalev, G., Klambauer, G., Hochreiter, S., and Nearing, G.: Towards learning universal, regional, and local hydrological behaviors via machine learning applied to large-sample datasets, Hydrology and Earth System Sciences, 23, 5089–5110, https://doi.org/10.5194/hess-23-5089-2019, 2019b.

Kratzert, F., Nearing, G., Addor, N., Erickson, T., Gauch, M., Gilon, O., Gudmundsson, L., Hassidim, A., Klotz, D., Nevo, S., Shalev, G., and Matias, Y.: Caravan - A global community dataset for large-sample hydrology, Scientific Data, 10, https://doi.org/10.1038/s41597-023-01975-w, 2023.

Kreienkamp, F., Philip, S. Y., Tradowsky, J. S., Kew, S. F., Lorenz, P., Arrighi, J., Belleflamme, A., Bettmann, T., Caluwaerts, S., Chan, S. C., Ciavarella, A., De Cruz, L., de Vries, H., Demuth, N., Ferrone, A., Fischer, E. M., Fowler, H. J., Goergen, K., Heinrich, D., Henrichs, Y., Lenderink, G., Kaspar, F., Nilson, E., Otto, F. E. L., Ragone, F., Seneviratne, S. I., Singh, R. K., Skålevåg, A., Termonia, P., Thalheimer, L., van Aalst, M., Van den Bergh, J., Van de Vyver, H., Vannitsem, S., van Oldenborgh, G. J., Van Schaeybroeck, B., Vautard, R., Vonk, D., and Wanders, N.: Rapid attribution of heavy rainfall events leading to the severe flooding in Western Europe during July 2021, Royal Netherlands Meteorological Institute (KNMI), 13, 18, https://www.worldweatherattribution.org/wp-content/uploads/Scientific-report-Western-Europe-floods-2021-attribution.pdf, accessed: 2023-12-31, 2021.

Kreklow, J., Tetzlaff, B., Burkhard, B., and Kuhnt, G.: Radar-based precipitation climatology in germany-developments, uncertainties and potentials, Atmosphere, 11, https://doi.org/10.3390/atmos11020217, 2020.

Lees, T., Buechel, M., Anderson, B., Slater, L., Reece, S., Coxon, G., and Dadson, S. J.: Benchmarking data-driven rainfall-runoff models in Great Britain: A comparison of long short-term memory (LSTM)-based models with four lumped conceptual models, Hydrology and Earth System Sciences, 25, 5517–5534, https://doi.org/10.5194/hess-25-5517-2021, 2021.

Lengfeld, K., Winterrath, T., Junghänel, T., Hafer, M., and Becker, A.: Characteristic spatial extent of hourly and daily precipitation events in Germany derived from 16 years of radar data, Meteorologische Zeitschrift, 28, 363–378, https://doi.org/10.1127/metz/2019/0964, 2019.

LfU-RLP - Rhineland-Palatine State Office for Environment: Discharge data Rhineland-Palatine, https://wasserportal.rlp-umwelt.de, accessed: 2022-03-02, 2022.

LIST - Luxembourg Institute of Science and Technology, Hydro-Climatological Observation network (HOST): Hourly Precipitation, 15-minute Discharge, https://envdata.private.list.lu/, accessed: 2022-04-01, 2022.

Liu, J., Koch, J., Stisen, S., Troldborg, L., Højberg, A. L., Thodsen, H., Hansen, M. F. T., and Schneider, R. J. M.: CAMELS-DK: Hydrometeorological Time Series and Landscape Attributes for 3330 Catchments in Denmark, Earth System Science Data Discussions, 2024, 1–30, https://doi.org/10.5194/essd-2024-292, 2024.

https://doi.org/10.5194/essd-2024-482
Preprint. Discussion started: 26 May 2025

Loritz, R., Dolich, A., Acuña Espinoza, E., Ebeling, P., Guse, B., Götte, J., Hassler, S. K., Hauffe, C., Heidbüchel, I., Kiesel, J., Mälicke, M., Müller-Thomy, H., Stölzle, M., and Tarasova, L.: CAMELS-DE: hydro-meteorological time series and attributes for 1555 catchments in Germany, Earth System Science Data Discussions, 2024, 1–30, https://doi.org/10.5194/essd-2024-318, 2024.

LVG - Landesamt für Vermessung und Geobasisinformation: Digitale Geländemodelle - Vermessungs- und Katasterverwaltung Rheinland-Pfalz, https://lvermgeo.rlp.de/geodaten-geoshop/open-data, accessed: 2024-05-25, 2021.

Mangukiya, N. K., Kumar, K. B., Dey, P., Sharma, S., Bejagam, V., Mujumdar, P. P., and Sharma, A.: CAMELS-INDIA: hydrometeorological time series and catchment attributes for 472 catchments in Peninsular India, Earth System Science Data Discussions, 2024, 1–43, https://doi.org/10.5194/essd-2024-379, 2024.

Marchi, L., Borga, M., Preciso, E., and Gaume, E.: Characterisation of selected extreme flash floods in Europe and implications for flood risk management, Journal of Hydrology, 394, 118–133, https://doi.org/10.1016/j.jhydrol.2010.07.017, 2010.

Mardhel, V., Pinson, S., and Allier, D.: Description of an indirect method (IDPR) to determine spatial distribution of infiltration and runoff and its hydrogeological applications to the French territory, Journal of Hydrology, 592, https://doi.org/10.1016/j.jhydrol.2020.125609, 2021.

Martínez-Carreras, N., Hissler, C., Gourdol, L., Klaus, J., Juilleret, J., Iffly, J. F., and Pfister, L.: Storage controls on the generation of double peak hydrographs in a forested headwater catchment, Journal of Hydrology, 543, 255–269, https://doi.org/10.1016/j.jhydrol.2016.10.004, 2016.

MECB - Ministère de l'Environnement, du Climat et du Développement durable & MEA - Ministère de l'énergie et de l'Aménagement du territoire: LIS-L Land Use 2018, https://data.public.lu/fr/datasets/lis-l-land-use-2007-2015-2018/, accessed: 2024-05-25, 2018.

MeteoLux: Precipitation data, https://www.meteolux.lu/de/klima/wetterstation/, accessed: 2024-06-23, 2024.

Meyer, J., Neuper, M., Mathias, L., Zehe, E., and Pfister, L.: Atmospheric conditions favouring extreme precipitation and flash floods in temperate regions of Europe, Hydrology and Earth System Sciences, 26, 6163–6183, https://doi.org/10.5194/hess-26-6163-2022, 2022.

Monteith, J. L.: Evaporation and environment, Symposia of the Society for Experimental Biology, 19, 205–234, 1965.

Muñoz Sabater, J.: ERA5-Land hourly data from 1981 to present, Copernicus Climate Change Service (C3S) Climate Data Store (CDS), https://doi.org/10.24381/cds.e2161bac, 2019.

Nijzink, J., Loritz, R., Gourdol, L., Zoccatelli, D., Iffly, J. F., and Pfister, L.: CAMELS-LUX: Highly Resolved Hydro-Meteorological and Atmospheric Data for Physiographically Characterized Catchments around Luxembourg [Data set]. Zenodo, https://doi.org/10.5281/zenodo.13846619, 2024.

Oudin, L., Hervieu, F., Michel, C., Perrin, C., and Andréassian, V.: Which potential evapotranspiration input for a lumped rainfall–runoff model? Part 2 – Towards a simple and efficient potential evapotranspiration model for rainfall–runoff modelling, Journal of Hydrology, 303, 290–306, https://doi.org/10.1016/j.jhydrol.2004.08.026, 2005.

Pardé, M.: Fleuves et rivières, Colin, Armand, Paris, 1947.

Penman, H. L.: Natural evaporation from open water, bare soil and grass, https://royalsocietypublishing.org/, 1947.

Pfister, L.: Hydrological processes in the Alzette river basin - On the potential and difficulties of interdisciplinary approaches in experimental hydrology, University of Strasbourg, p. 128, 2012.

Pfister, L., Humbert, J., and Hoffmann, L.: Recent trends in rainfall-runoff characteristics in the Alzette river basin, Luxembourg, Climatic Change, 45, 323–337, https://doi.org/10.1023/A:1005567808533, 2000.

Pfister, L., Wagner, C., Vansuypeene, E., Drogue, G., and Hoffmann, L.: Atlas climatique du grand-duché de Luxembourg, Musée national d'histoire naturelle, Société des naturalistes luxembourgeois, Centre de recherche public Gabriel Lippmann, Administration des services techniques de l'agriculture, Luxembourg, ISBN: 2-919877-24-0, ISBN 2-919877-24-0, 2005.

Pfister, L., Martínez-Carreras, N., Hissler, C., Klaus, J., Carrer, G. E., Stewart, M. K., and McDonnell, J. J.: Bedrock geology controls on catchment storage, mixing, and release: A comparative analysis of 16 nested catchments, Hydrological Processes, 31, 1828–1845, https://doi.org/10.1002/hyp.11134, 2017.

Pfister, L., Faber, O., Hostache, R., Iffly, J. F., Matgen, P., Minette, F., Trebs, I., Bastian, C., Göhlhausen, D., Meisch, C., and Patz, N.: Crue éclair du 22 juillet 2016 dans la region de Larochette - Étude méchanistique et fréquentielle réalisée en 2018 pour le compte de l'Administration de la gestion de l'eau, Tech. rep., Administration de la gestion de l'eau, Esch-sur-Alzette, https://eau.gouvernement.lu/dam-assets/publications/crue-éclair-du-22-juillet-2016/1812-LIST-BrochureCrueEclair.pdf, accessed: 2023-12-30, 2018.

Pfister, L., Douinot, A., Hostache, R., Iffly, J. F., Matgen, P., Minette, F., Bastian, C., Gilbertz, C., Göhlhausen, D., Meisch, C., and Patz, N.: Crues subites 2018 - Étude méchanistique et fréquentielle des crues subites de 2018 au Luxembourg, Tech. rep., Administration de la gestion de l'eau, Esch-sur-Alzette, https://eau.gouvernement.lu/fr/services-aux-citoyens/publications/2021/brochures/Crues-subites-2018.html, accessed: 2023-12-30, 2020.

Pöschmann, J. M., Kim, D., Kronenberg, R., and Bernhofer, C.: An analysis of temporal scaling behaviour of extreme rainfall in Germany based on radar precipitation QPE data, Natural Hazards and Earth System Sciences, 21, 1195–1207, https://doi.org/10.5194/nhess-21-1195-2021, 2021.

Robinson, J. S., Sivapalan, M., and Snell, J. D.: On the relative roles of hillslope processes, channel routing, and network geomorphology in the hydrologic response of natural catchments, Water Resources Research, 31, 3089–3101, https://doi.org/10.1029/95WR01948, 1995.

Sappington, J. M., Longshore, K. M., and Thompson, D. B.: Quantifying Landscape Ruggedness for Animal Habitat Analysis: A Case Study Using Bighorn Sheep in the Mojave Desert, The Journal of Wildlife Management, 71, 1419–1426, https://doi.org/10.2193/2005-723, 2007.

Schmithüsen, J.: Das Klima in Das Luxemburger Land - Landesnatur, Volkstum und bäuerliche Wirtschaft, S. Hirzel, Leipzig, 1940.

SPW - Service Public de Wallonie: Relief de la Wallonie - Modèle Numérique de Terrain (MNT) 2013-2014, https://geoportail.wallonie.be/catalogue/6029e738-f828-438b-b10a-85e67f77af92.html, accessed: 2024-05-25, 2014.

Taszarek, M., Allen, J. T., Brooks, H. E., Pilguj, N., and Czernecki, B.: Differing trends in United States and European Severe Thunderstorm Environments in a Warming Climate, Bulletin of the American Meteorological Society, 102, E296–E322, https://doi.org/10.1175/BAMS-D-20-0004.1, 2021.

Uhan, J., Andjelov, M., Mardhel, V., and Frantar, P.: Index of development and persistence of the river networks (IDPR) as a component of regional groundwater vulnerability assessment in Slovenia., Proceedings on the International Conference on Groundwater vulnerability assessment and mapping. Ustron, Poland, pp. 15–18, 2004.

Winterrath, T., Brendel, C., Hafer, M., Junghänel, T., Klameth, A., Lengfeld, K., Walawender, E., Weigl, E., and Becker, A.: RADKLIM Version 2017.002: Reprocessed quasi gauge-adjusted radar data, 5-minute precipitation sums (YW), Tech. rep., German Weather Service (DWD), https://doi.org/10.5676/DWD/RADKLIM_YW_V2017.002, 2018.

Wrede, S., Fenicia, F., Martínez-Carreras, N., Juilleret, J., Hissler, C., Krein, A., Savenije, H. H. G., Uhlenbrook, S., Kavetski, D., and Pfister, L.: Towards more systematic perceptual model development: a case study using 3 Luxembourgish catchments, Hydrological Processes, 29, 2731–2750, https://doi.org/10.1002/hyp.10393, 2015.